Bluff Bodies and Wake-Wall Interactions

Mark C. Thompson,[1] Thomas Leweke,[2] and Kerry Hourigan[1]

[1]Department of Mechanical & Aerospace Engineering, Monash University, Clayton, VIC 3800, Australia; email: mark.thompson@monash.edu
[2]IRPHE (Institut de Recherche sur les Phénomènes Hors Equilibre), CNRS, Aix-Marseille Université, Centrale Marseille, 13384 Marseille, France

Annu. Rev. Fluid Mech. 2021. 53:1–30

The *Annual Review of Fluid Mechanics* is online at fluid.annualreview.org

https://doi.org/10.1146/annurev-fluid-000000-000000

Keywords

bluff bodies, wall interactions, wake transitions, flow stability, solid-solid contact

Abstract

This article reviews the dramatic variation in wake structures and flow transitions, in addition to body forces, that appears as the motion of bluff bodies through a fluid occurs increasingly closer to a solid wall. In particular, the two cases of bluff bodies translating parallel at varying heights to solid walls and bluff bodies impacting on solid walls are discussed. In the former case, the changes to the wake structures as the flow varies from that of an isolated body to that of a body on or very close to the wall are highlighted, including the effects when the body is rotating. For the latter case of an impacting body, the flow structures following impact and their transition to three-dimensionality are reviewed. The issue of whether there is solid-solid contact between the bluff body and a wall and its importance to body motion is discussed.

1. INTRODUCTION

The flow around generic bluff bodies, such as circular cylinders and spheres, has been studied for more than a century. The vortex-shedding phenomenon occurring in the wake of these bodies, and the associated fluid-structure interactions, have been the topic of a number of previous contributions to the Annual Review of Fluid Mechanics: Berger & Wille (1972), Bearman (1984), Oertel (1990), Williamson (1996b), Williamson & Govardhan (2004), Choi et al. (2008), Ern et al. (2012).

Building on and extending these reviews, this article focuses on the wake dynamics of generic bluff bodies when moving relative to, and interacting with, walls. Examples of the wakes generated by a cylinder rolling on a wall and a sphere impacting a wall are shown in **Figure 1**. These vortical flows bear little resemblance to the wakes of isolated cylinders and spheres in freestream.

1.1. Practical Significance

A solid body moving along or colliding with a solid surface is a common element relevant to many industrial and environmental processes, leading to complex energy exchanges. An example is the resuspension of particles deposited on a surface, such as dust on the ground or sediments in rivers, by the wake generated by the impact of an object or other particles; see, e.g., Willetts 1998 and Ziskind 2006, for reviews on this topic - also see **Figure 1*b***. Wear due to particle impacts on surfaces is a major problem in many areas, including pumping and processing of slurry flows (Clark 1992), as is the damaging impact of small particles on high-technology equipment in desert environments (Yildirim et al. 2017). Micrometer-

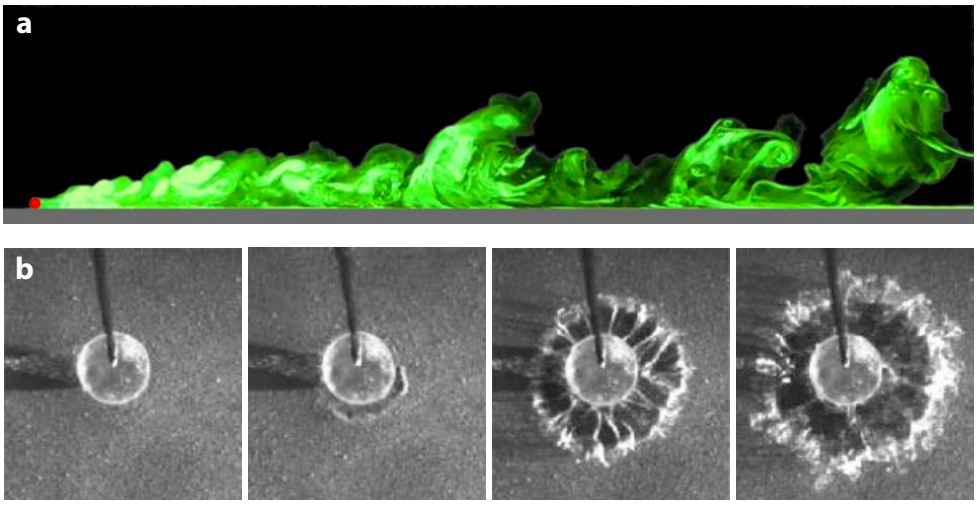

Figure 1

(*a*) Mixing induced by a cylinder (red circle on the left) rolling in a quiescent fluid along a wall previously coated with a thin layer of dyed fluid. Experimental visualization in water at $Re = 220$. (*b*) Resuspension of a layer of particles by the normal wall impact of a sphere at $Re = 3100$. Oblique view from above. Panel *b* reprinted from Eames & Dalziel (1999), with permission of AIP Publishing.

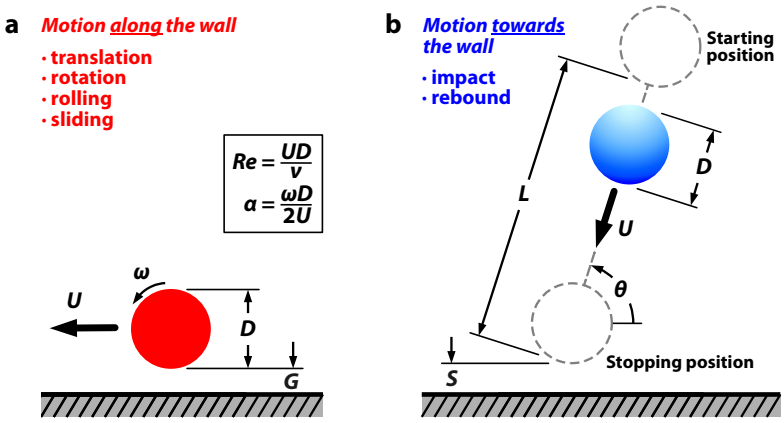

Figure 2

Schematics of the two types of configurations considered in this review, including the main parameters: (*a*) a bluff body translating and rotating along a wall, separated by a gap G; and (*b*) a body, initially at rest, moving a distance L before stopping at or near a wall (without or with rebound). In all cases the fluid is stationary with respect to the wall.

scale solid particles are used in a range of processes – polishing, shot peening, sand blasting and kinetic consolidation processes – in industries such as metallurgy and pharmaceutical manufacturing. At a larger scale, many sports, such as football, cricket, baseball, snooker, pétanque, bowls, tennis and table tennis, and golf, to name but a few, involve bluff bodies that move near and on a surface, and where impact, rolling, spin, and bounce are important.

1.2. The Problem of Solid-to-Solid Contact

Sisyphus, according to Greek mythology, was condemned to eternally repeat the process of rolling a massive boulder up a hill, only for it to then roll down the hill again (Homer 9th-8th century BC). Were we to model this process by a perfectly smooth sphere and hill within an incompressible Newtonian atmosphere, a startling result would await – no matter how mightily Sisyphus may strain, the sphere would not budge, even on a steep slope, due to infinite resistive pressure forces near the point of contact. This is the so-called Rolling Paradox (see section 4.3). However, of course bodies do roll, with the first scientific study initially published in 1632 by Galileo with his famous rolling-sphere experiments (Galilei 1638).

Galileo was reputed, anecdotally, to have dropped spheres from the Tower of Pisa to show that acceleration was proportional to gravitational force, independent of mass. However, for a perfectly smooth ball and ground and an incompressible Newtonian atmosphere, the dropped spheres would never actually touch the ground, due to the infinite fluid forces in the small gap as the sphere approaches the solid surface (Brenner 1961). And yet solid-to-solid impact of dropped bodies are evidently observed (and heard).

When isolated from a wall, the identical assumptions for a body moving relative to a the fluid does allow accurate modelling of the body and its wake (e.g., Johnson & Patel 1999, Thompson et al. 1996). Therein lies a major challenge to understanding the seemingly simple problem of a body in a fluid moving near, or impacting on, a wall.

1.3. Scope of Review

This review focuses on the flow around the generic bluff bodies of a circular cylinder and sphere, showing how the characteristics of the wake change due to the presence of the wall under a variety of translation, rotation, rolling, and impact conditions, and the effects of Reynolds number – see **Figure 2** for the setups and important parameters. At present, the results of past investigations are often scattered throughout various research subfields, not always cross-referenced and sometimes inaccurate – this review aims to provide an overview of these various studies, raising important questions still to be fully addressed. The focus is on bodies translating in otherwise stationary fluids with fixed walls. The issue of fluid-structure interaction, and specifically flow-induced vibration, is limited to a brief discussion concerning freely rolling bodies. Most of the referenced results were obtained from experiments in water channels or tanks, or in computational studies involving direct numerical simulations. Comparisons between the two are shown where possible.

The starting point is a brief review of the wake transitions of generic bluff bodies (2-dimensional cylinder and 3-dimensional sphere) at significant distances from a wall, considering both non-rotating and rotating cases, as wall as impulsively arrested bodies, in order to provide some context. Then, we map the changes in wakes as the bodies are located increasingly closer to a wall. Finally, we review the issues of bluff-body contact with a wall and point out future directions on this topic.

2. UNIFORMLY TRANSLATING ISOLATED BLUFF BODIES

2.1. Non-rotating Bodies

2.1.1. Circular cylinders. The flow past a circular cylinder has been a generic fluid flow problem that has maintained continuing interest for more than a century, and the intricate experimental and mathematical details of the transitions leading towards a fully turbulent wake have been revealed especially over the last three decades. The initial transition at Reynolds number $Re_{C_1} \approx 46$ occurs through a Hopf bifurcation from a symmetric pair of attached recirculation bubbles to a periodic two-dimensional Bénard-von Kármán (BvK) wake (Dušek et al. 1994, Williamson 1989), see **Figure 3*a***. Here, the Reynolds number is based on the free-stream velocity (U) and the cylinder diameter (D): $Re = UD/\nu$ (ν is the kinematic viscosity of the fluid). On increasing the Reynolds number, the wake next undergoes a subcritical (hysteretic) three-dimensional transition at $Re_{C_2} \approx 190$ (Barkley & Henderson 1996, Williamson 1996a,b), which manifests as a sinusoidal distortion of the spanwise vortex rollers with streamwise vortex structures connecting these. At onset, the spanwise wavelength (λ) is approximately four cylinder diameters, and this wake instability is commonly known as Mode A. On increasing the Reynolds number further, another three-dimensional mode of much shorter spanwise wavelength ($\lambda \approx D$), Mode B, becomes unstable at $Re_{C_3} \approx 260$. The remnants of this mode appear to persist at much higher Reynolds numbers after the wake becomes fully chaotic (Henderson 1997, Williamson 1996a,b). The characteristic three-dimensional modes are visualized in **Figure 3*b***. Of interest, equivalent modes have also been recognised in the wakes of other two-dimensional cylindrical bodies, such as square cylinders (Robichaux et al. 1999) and angled airfoils (He et al. 2017). However, different modes can be important for other cylindrical geometries; e.g., a quasiperiodic mode is the first transition mode of a normal-flat-plate wake (Thompson et al. 2006b).

Hopf bifurcation: loss of stability of a steady state, giving rise to a periodic solution, as the control parameter is increased

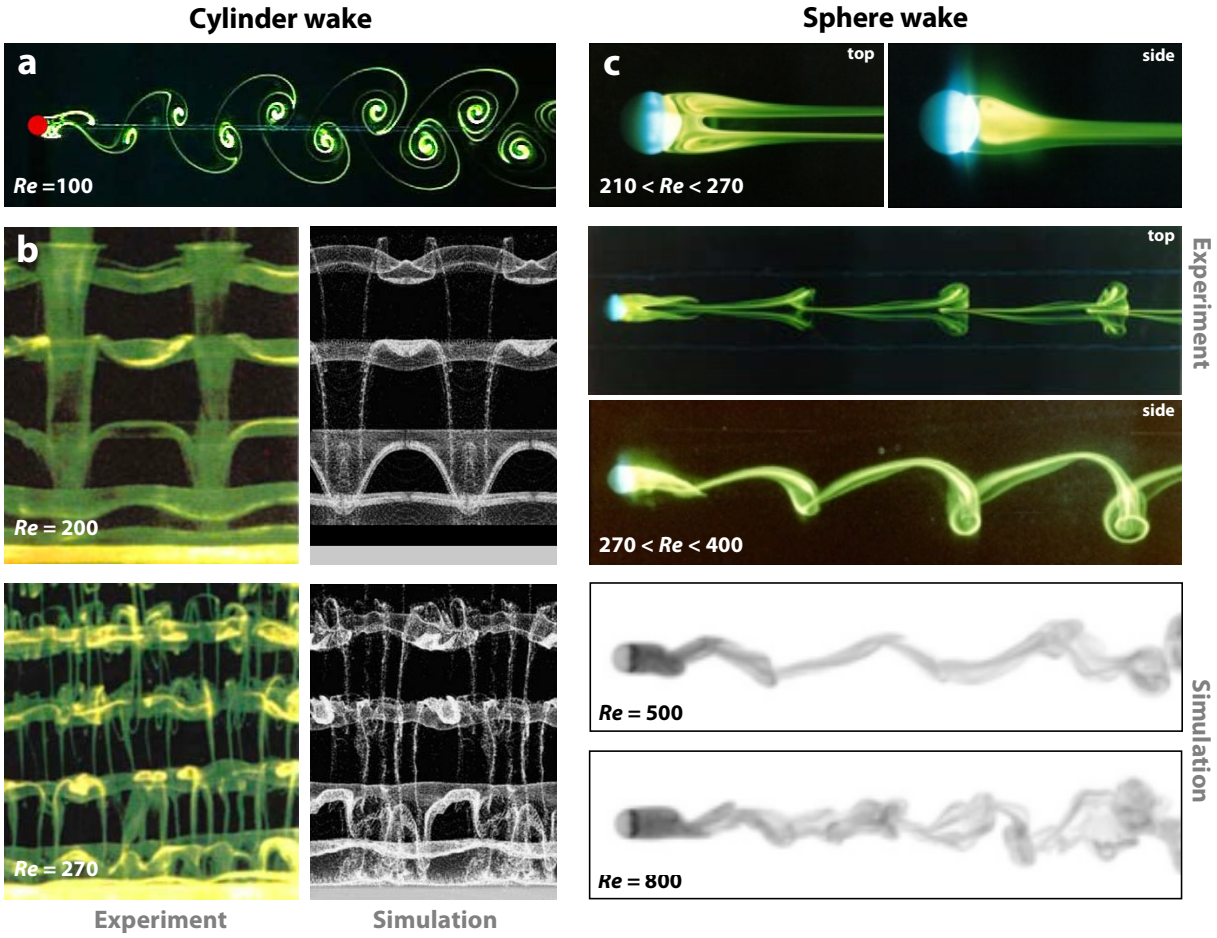

Figure 3

(*a*) Two-dimensional periodic cylinder wake (experimental dye visualization). (*b*) Three-dimensional structures in the wake of a cylinder (flow is upward, the cylinder is at the bottom). Top: Mode A, bottom: Mode B, left: dye visualization, right: numerical simulation with tracer particles. Panel *b* (left) adapted with permission from Williamson (1996a); panel *b* (right) adapted from Thompson et al. (2006b), with permission from Elsevier. (*c*) Evolution of the wake of a sphere with increasing Reynolds number (dye visualization and numerical simulation). Experimental top views in panel *c* reproduced from Thompson et al. (2001), with permission from Elsevier.

2.1.2. Spheres. The sequence of wake modes for a sphere, as Re is increased, is illustrated in **Figure 3*c***. Consistent with other studies (Tomboulides & Orszag 2000, Ghidersa & Dušek 2000, Thompson et al. 2001), experiments and numerical computations performed by Johnson & Patel (1999) found that the initial axisymmetric wake undergoes a regular (i.e., steady→steady) bifurcation through an off-axis shift of the steady axisymmetric recirculating bubble at $Re_{S_1} \approx 210$. This results in a double-threaded wake consisting of a trailing vortex pair, as observed previously for buoyant oil drops (Magarvey & Bishop 1961a,b). On further increasing Re, a second topological transition from the steady two-threaded wake to a periodic wake occurs at $Re_{S_2} \approx 270$ (above references), with the trailing vortices form-

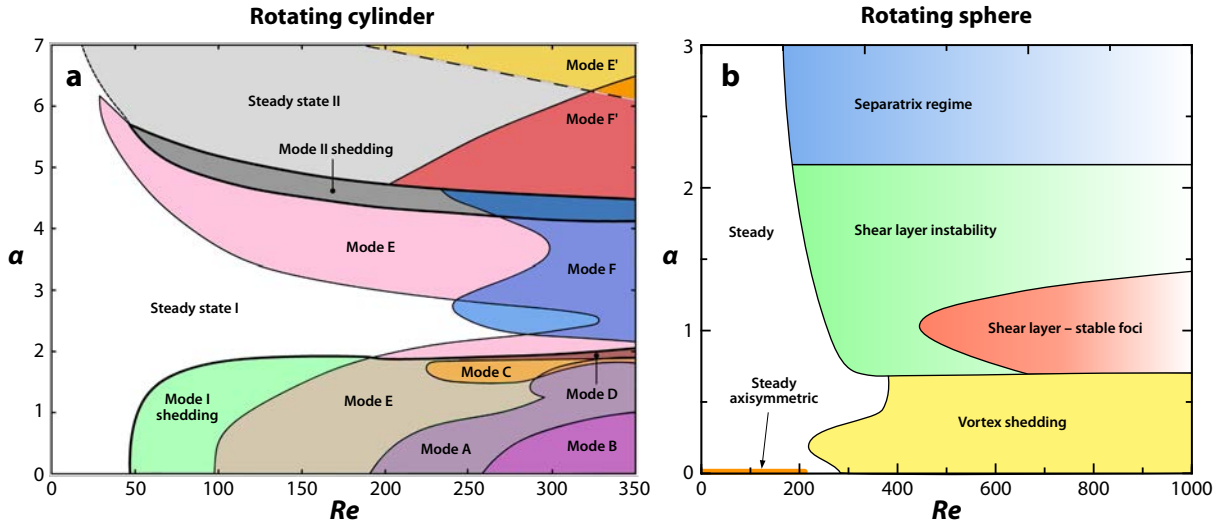

Figure 4

(*a*) Stability diagram in Re–α parameter space for a rotating cylinder. Panel *a* adapted from Rao et al. (2015b), with permission from Elsevier. (*b*) Wake regimes of a rotating sphere, as function of Re and α, based on data collected by Poon et al. (2014) and Dobson et al. (2014).

ing kinks that develop into strongly skewed loops advecting downstream. Computations by Mittal (1999) and experiments of Brücker (2001) showed that the vortex loops in the wake lose planar symmetry at $Re_{S_3} \approx 400$. These vortex loops are maintained at much higher Reynolds numbers, despite an increasing chaotic component. Through large-eddy simulations, Chomaz et al. (1993) and Tomboulides & Orszag (2000) reported fine-scale wake flow structures for $500 < Re < 1000$; they speculated that these develop from a Kelvin-Helmholtz instability of the shear layer separating from the sphere. In agreement, Magarvey & Bishop (1961b) experimentally observed a breakdown in periodicity of the hairpin shedding for $Re > 600$. The same shear layer instability manifests in a cylinder wake beyond $Re \approx 2000$, (see, e.g., Prasad & Williamson 1997, Thompson & Hourigan 2005), although, for experiments at least, the onset is dependent on background turbulence.

2.2. Rotating Bodies

2.2.1. Circular cylinders. Numerical and experimental investigations have characterised and quantified the wake of a rotating cylinder for rotation rates $\alpha \leq 7$ and Reynolds numbers $Re \leq 400$ – see **Figure 4*a***. Here, α is the ratio of the circumferential speed of the cylinder surface and the flow velocity, or equivalently the cylinder translation speed: $\alpha = \omega D/(2U)$, with ω the angular velocity of the body. Using linear stability analysis, various two- and three-dimensional transitions have been identified and mapped. This effectively extends the previously described results for a non-rotating cylinder (section 2.1.1) from the $\alpha = 0$ axis into the Re-α parameter space. For small rotation rates ($\alpha \lesssim 2$), the rotation breaks the symmetry of the BvK wake, but essentially only perturbs the vortex shedding and transition modes (A and B). However, as the rotation rate approaches $\alpha = 2$, the connection points at the cylinder of the upstream and downstream stagnation streamlines essentially merge,

significantly altering the flow topology, so that shedding is increasingly suppressed. At even higher rotation rates, these two streamlines join and separate from the surface of the cylinder forming a closed region of pure rotation about the cylinder. Given this change to the underlying base flow with α, the parameter space can be broadly split into two regions: $\alpha < 2$ and $\alpha > 2$, as the parameter map of **Figure 4*a*** shows. Two unsteady two-dimensional regimes exist: Mode I shedding occurs for $\alpha \lesssim 2$ and is characterised by alternate vortex shedding, while Mode II shedding only occurs over a small range of α, at much higher rotation rates that result in single-sided vortex shedding (see, e.g., Stojković et al. 2002, 2003, Mittal & Kumar 2003). Two steady flow regimes have also been identified (Mittal & Kumar 2003, Pralits et al. 2010, Rao et al. 2015b): Steady state I occurs at lower Re, while Steady state II manifests at higher rotation rates beyond the Mode II shedding region. These two states are distinguished by differences in flow features such as the drag coefficient and the location of stagnation points. At higher Re, a variety of unstable three-dimensional modes with different spanwise wavelengths is found, including a periodic subharmonic mode (C), which is also found in other asymmetric bluff body flow configurations, such as curved circular cylinders (rings) or inclined square cylinders (Sheard et al. 2005, Sheard 2011), and a steady three-dimensional mode (E).

Subharmonic: having half the frequency of the base flow

2.2.2. Spheres. Previous numerical investigations (Kim 2009, Giacobello et al. 2009, Poon et al. 2014, Dobson et al. 2014, Rajamuni et al. 2018) on the effects of rotation on the wakes of rigidly mounted rotating spheres at low Reynolds numbers ($Re \leq 1000$) have revealed considerable wake modifications and even suppression of the vortex shedding, depending on rotation rate. In comparison with the cylinder case, the wake structure is more strongly affected at lower rotation rates, with **Figure 4*b*** showing that a broad change occurs beyond $\alpha \simeq 0.7$. Similar to the cylinder, in the rotation centerplane, high rotation causes the streamlines to bend around the sphere, again leading to an isolated region of co-rotation near the sphere surface (separatrix regime).

2.3. Impulsively Arrested Bodies

2.3.1. Circular cylinders. The flow evolution associated with an arresting body has received little attention to date, a few notable studies include those by Tatsuno & Taneda (1971), Wang & Dalton (1991) and Sheard et al. (2007) for the case of an arresting cylinder. They showed that, during cylinder motion, a recirculating wake develops and grows behind the body, consisting of an attached counter-rotating vortex pair. After the cylinder is impulsively stopped, the momentum in the surrounding fluid carries the wake over the cylinder, and the shear at the surface induces secondary vortices that pair with the primary wake vortices as the latter pass the cylinder (**Figure 5*a***). In the subsequent flow evolution, Sheard et al. (2007) found that, similar to the flow past an arresting sphere discussed below, these counter-rotating vortex pairs self-propel over a range of sometimes surprising trajectories. For low Reynolds numbers and short translation distances, the wake vortices move past the cylinder and continue in the direction of the original cylinder motion. For higher Reynolds numbers, the pairs deviate outwards in circular arcs of increasing curvature, even to the extent that they can actually collide behind the cylinder. The curvature depends on the circulation balance of the vortex pairs. At sufficiently large translation distances, a wake instability that would lead to vortex shedding breaks the reflective symmetry about the centerline of the wake.

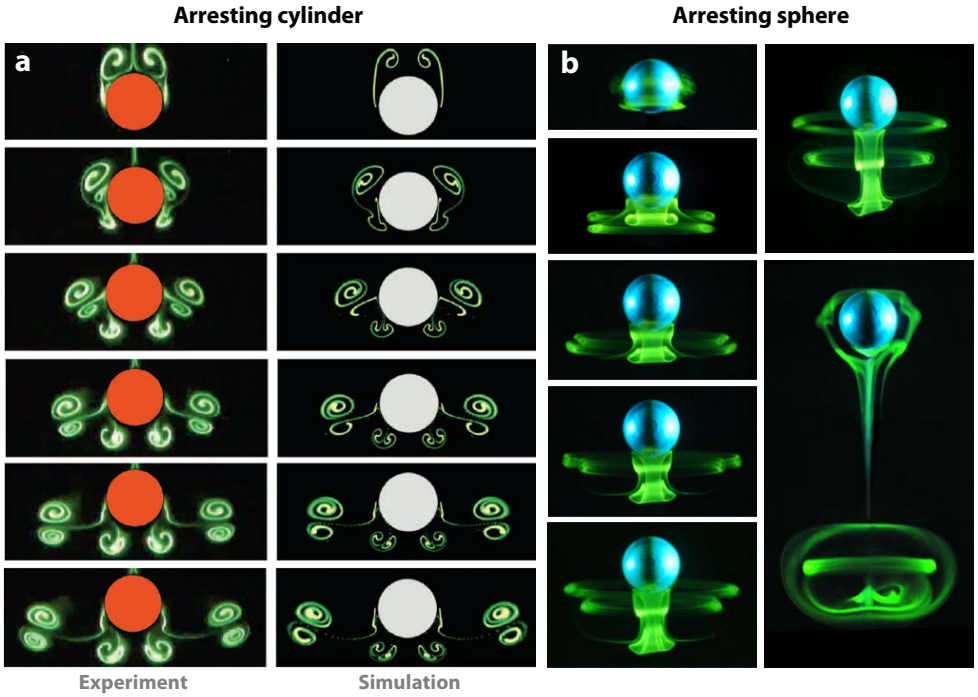

Figure 5

(*a*) Flow around an impulsively arrested cylinder previously translating a distance $2D$ from top to bottom at $Re = 500$; experimental dye visualization (left) and numerical simulation with tracer particles (right). Panel adapted from Sheard et al. (2007), with permission of AIP Publishing. (*b*) Experimental dye visualization of the vortex rings developing for an impulsively arrested sphere after translating a distance $5D$ at $Re = 800$.

2.3.2. Spheres. Leweke et al. (2004a) and Thompson et al. (2007) have investigated the flow dynamics of an impulsively arrested sphere. For an arrest occurring in isolation (**Figure 5*b***), the recirculating wake translates towards the arrested sphere before spreading laterally as a vortex ring in the original upstream direction. A second vortex ring of opposite sign is induced from the sphere surface and pairs with the primary ring. The vortex ring pair follows a loop trajectory due to mutual induction, after which the primary ring continues its upstream motion, whereas the secondary ring is left behind and fades out.

3. BLUFF BODIES MOVING PARALLEL TO A WALL

3.1. Circular Cylinders

Taneda (1965) was one of the first to visualize the wake of a circular cylinder moving parallel to a wall. He specifically examined the change to the vortex street as the gap height was reduced from $G/D = 0.6$ to 0.1 (see **Figure 2*a***) at $Re = 170$. For the smaller gap, it appeared that only a single row of vortices formed, with the individual vortices being unstable and decaying rapidly. The streamwise wavelength of the vortex street increased as the gap was reduced.

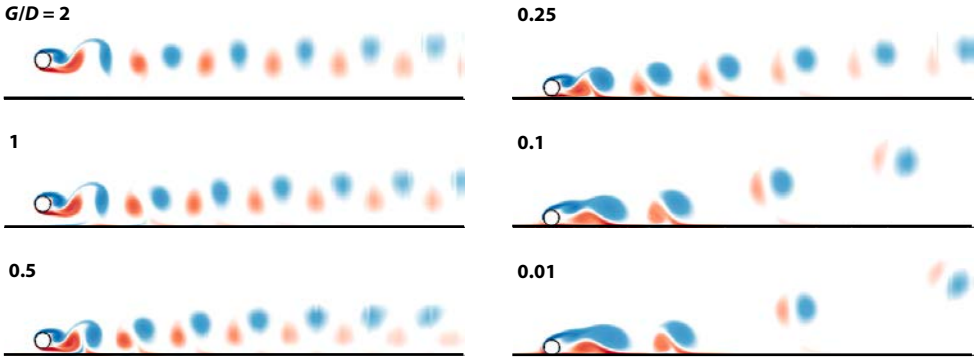

Figure 6

Two-dimensional wakes (vorticity fields) of cylinders translating parallel to a solid wall at different gaps G, for $Re = 200$. Figure adapted from Rao et al. (2013a), with permission from Elsevier.

Various authors have since investigated the effect of wall proximity at low Reynolds numbers through two-dimensional numerical simulations. For example, for non-rotating cylinders, Huang & Sung (2007) quantified the wake and forces for $0.1 \leq G/D \leq 1$ and for $Re \leq 600$, while Yoon et al. (2010) considered the effect of gap height at $Re = 200$. A change from the standard BvK wake to a wake dominated by one-sided shedding was found to occur at $G/D \approx 0.25$. Also, the shedding frequency f, expressed as the non-dimensional Strouhal number $St = fD/U$, initially increases slightly as the gap is reduced towards $G/D = 0.5$, but it decreases rapidly beyond this point, which is consistent with Taneda's (1965) observation of an increased wavelength. The higher blockage to fluid passing under the cylinder, as the wall gap is reduced, tends to stabilize the wake to the onset of periodic shedding, resulting in an increase in the critical Reynolds number from $Re_{C_1} = 46$ for $G/D \to \infty$ to $Re_{C_1} > 100$, for gaps below $G/D \lesssim 0.4$.

More recently, Rao et al. (2013a, 2015a) simulated the flow past non-rotating and rotating circular cylinders moving through a fluid at different heights above a no-slip plane boundary for $Re \leq 400$. The series of two-dimensional vorticity fields in **Figure 6** shows in more detail the changes to the flow physics caused by wall proximity. As the gap gets smaller, the increasing blockage reduces the circulation fed into the lower vortices shedding into the wake, affecting the symmetry between positive and negative vortices forming the vortex street. In addition, for small gaps, the proximity of the upper shed vortices to the wall induces opposite-signed secondary vorticity there that can be advected into the wake to pair with the primary vortices. Thus, the character of the wake changes as the gap is reduced, and with it the nature of the first transition from steady two-dimensional flow. Whereas this transition occurs through a Hopf bifurcation to periodic flow at large gaps, a regular bifurcation leads to steady three-dimensional flow (Mode E) for small gaps. Similarly, the onset of the three-dimensional Mode A instability, and indeed whether it is the first three-dimensional instability, is very sensitive to gap size.

Figure 7 summarizes the various transitions and unstable wake modes for cylinders moving along a wall, as function of Reynolds number and gap size, and also for the cases with simultaneous forward or backward rotation. Gap size has a strong influence in the range $G/D \lesssim 0.4$; for higher values, the transition sequence is close to that of an isolated cylinder. Some of the three-dimensional instability modes are depicted in **Figure 8**. As

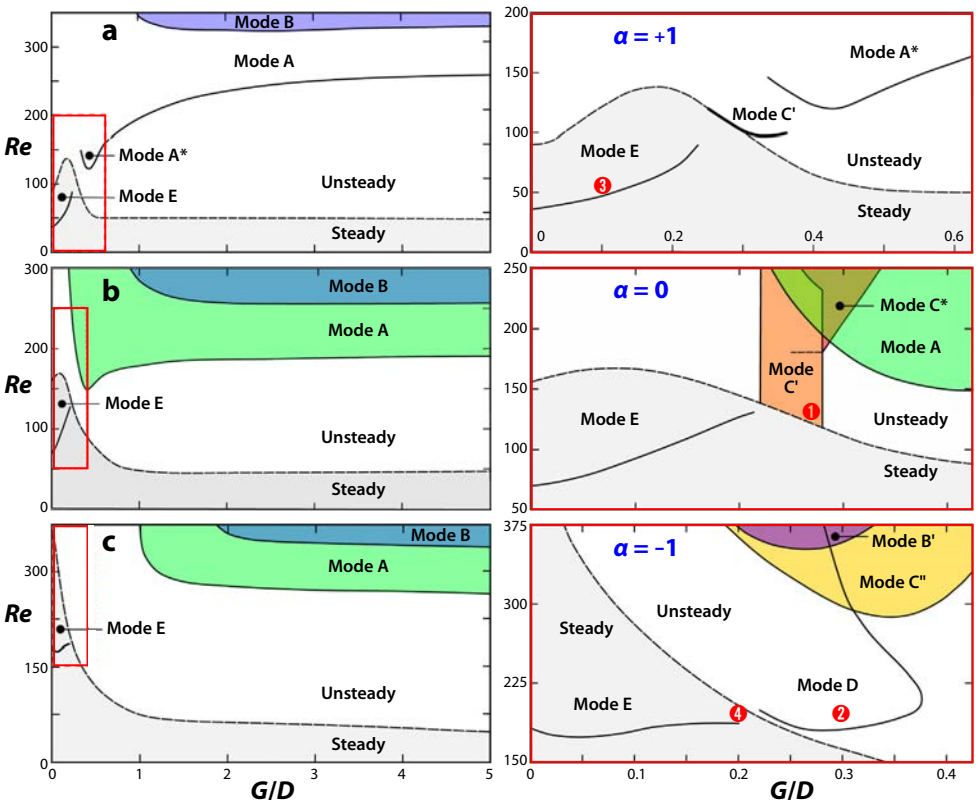

Figure 7

Parameter space showing the wake modes of a cylinder translating near a wall, for (*a*) forward (normal) rotation, (*b*) no rotation and (*c*) backward (reverse) rotation. The transition from steady to unsteady flow is marked by a dashed line. Diagrams on the right are enlargements of the regions outlined in red on the left. Numbers in red refer to the modes shown in **Figure 8**. Figure adapted from Rao et al. (2015a), with permission from Elsevier.

for the isolated cylinder, they include a subharmonic mode (Mode C'), as well as a steady three-dimensional mode (E) at different spanwise wavelengths.

3.2. Spheres

Prograde rotation: rotation in the same direction as for rolling without slip

Amongst studies conducted on rotating spheres near boundaries are the works of Zeng et al. (2005) and Cherukat & McLaughlin (1994), the latter being restricted to the Stokes regime, where a sphere is moving parallel to a wall at a distance of 0.25 sphere diameters or greater, and is free to rotate. Their results indicate that, in general, any observed induced rotation is in the prograde direction and that this rotation has little effect on the lift and drag forces.

The transition to unsteady flow with hairpin vortices and loops in the wake occurs earlier than for an isolated sphere, with the critical Reynolds number decreasing as the distance to the wall is reduced. At the lowest gap ratio tested ($G/D = 0.25$), a sudden increase is observed: the wake remains steady beyond $Re = 300$. Zeng et al. (2005) find that this delay

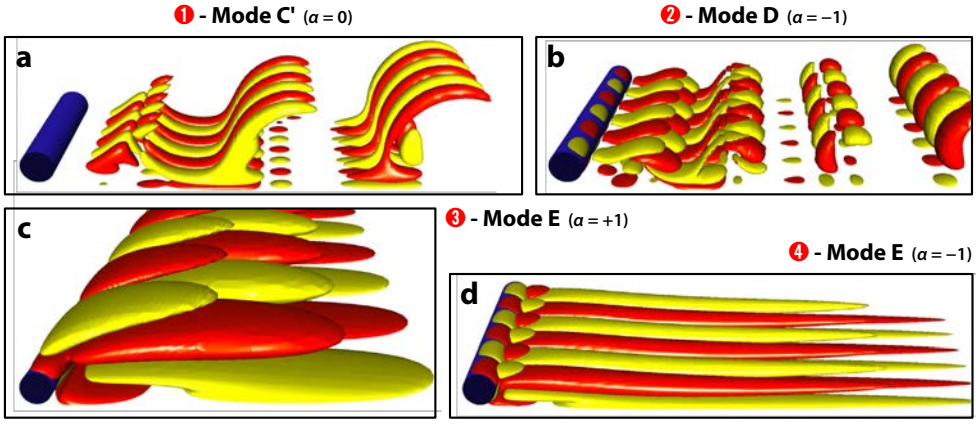

Figure 8

Three-dimensional instability modes of the wake of a cylinder translating parallel to a wall, visualized by isosurfaces of positive and negative streamwise vorticity. (*a*) Subharmonic Mode C' with $\lambda/D = 1.35$ for the sliding cylinder. (*b*) Periodic Mode D with $\lambda/D = 2.6$ for the cylinder in reverse rotation. (*c*) Steady Mode E with $\lambda/D = 11$ for the cylinder in normal rotation. (*d*) Steady Mode E with $\lambda/D = 2.75$ for the cylinder in reverse rotation. Numbers in red refer to the locations in the parameter space shown in **Figure 7**. Figure adapted from Rao et al. (2015a), with permission from Elsevier.

of unsteadiness at small gaps is caused by viscous effects of the nearby wall, as well as by the strong asymmetry of the flow configuration.

The behaviour of the lift and drag coefficients of spheres translating close to a wall was investigated by Zeng et al. (2009) at moderate Reynolds numbers covering the steady regimes ($Re < 300$). Force coefficients for spheres are defined in the standard way though $F = C_F \cdot \frac{1}{2}\rho U^2 \cdot \frac{\pi}{4}D^2$, where F is the corresponding force and ρ the fluid density. These force coefficients, as a function of Reynolds number and gap ratio, are summarized in **Figure 9** for the case of pure translation, as predicted by Zeng et al. (2009) and others. The isolated sphere drag variation, together with predictions of lubrication theory, are also provided for comparison. Orders-of-magnitude changes in both the drag and lift coefficients are observed as the Reynolds number and gap ratio are varied, the latter showing the profound effect of the wall. Note that the lift remains finite for all parameter values, whereas the drag diverges logarithmically and as Re^{-1} for vanishing gap size and Reynolds number, respectively.

Lubrication theory: modelling of the flow in a thin fluid layer bounded by solid surfaces, neglecting inertial effects

4. BLUFF BODIES ROLLING ALONG A WALL

4.1. Rolling Circular Cylinders

As discussed in section 3.1, the immediate proximity of a wall suppresses the passage of fluid underneath the cylinder, leading to single-sided vortex shedding into the wake. In turn, the proximity to the wall of these shed vortices induces secondary wall vorticity, which separates and rolls up into weaker vortex structures that pair with the primary vortices to form the wake. The addition of prograde (normal) rolling to the scenario has two main effects: it increases the circulation fed into the upper primary vortices (because of the increased velocity gradient at the cylinder surface), and it also leads to separation

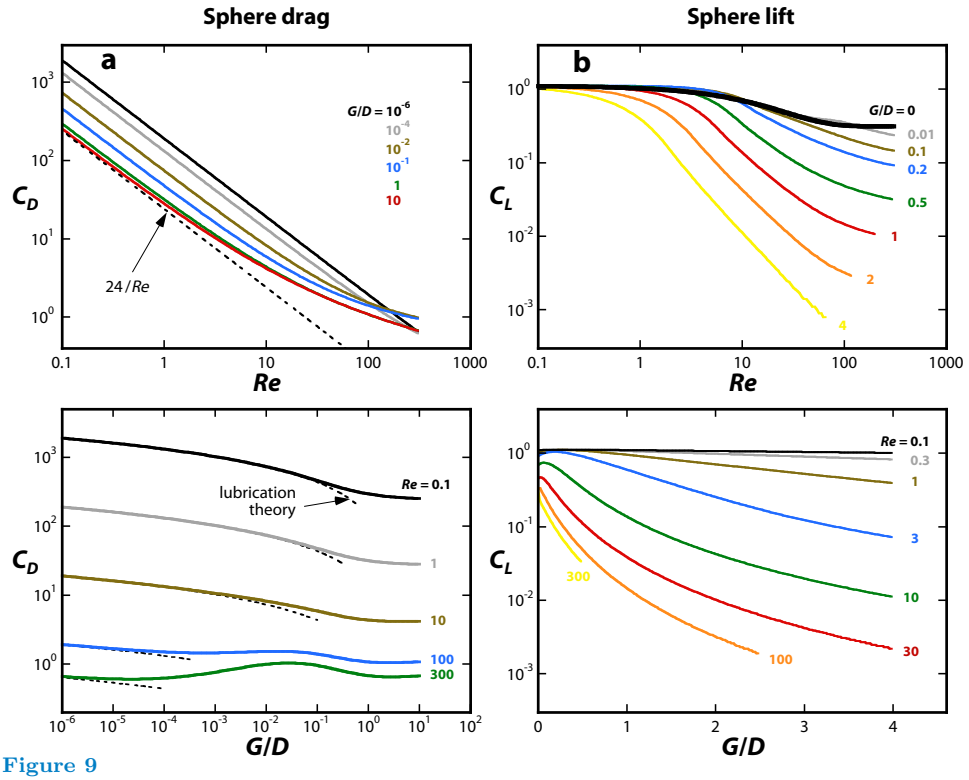

Figure 9

(*a*) Drag and (*b*) lift coefficients for a non-rotating sphere moving parallel to a solid wall in a quiescent fluid, as function of Reynolds number (top) and of gap size (bottom). The limits for Stokes flow at large gaps and for lubrication at vanishing gaps (Goldman et al. 1967) are shown as dashed lines. Diagrams computed using the correlations proposed by Zeng et al. (2009), based on a survey of various experimental and numerical studies.

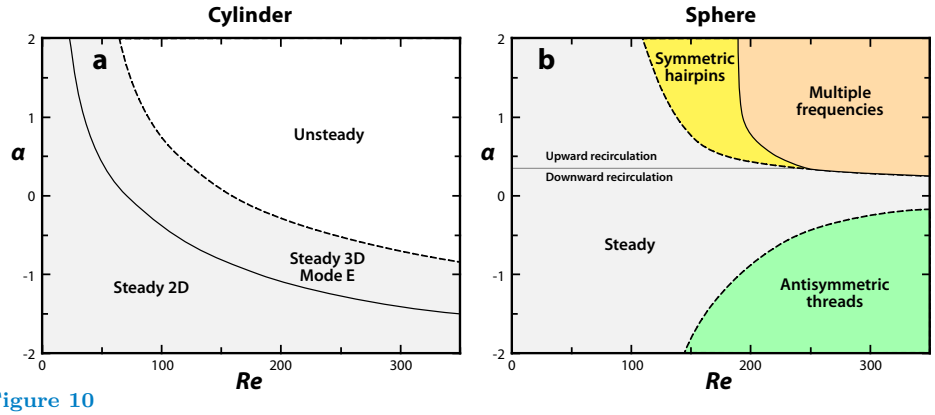

Figure 10

Wake regimes for (*a*) a cylinder and (*b*) a sphere translating along a wall and rotating at different rates. The gap size is $G/D = 0.005$. Diagrams based on results from numerical simulations and stability analyses by Stewart et al. (2010a,b) and Rao et al. (2011, 2012).

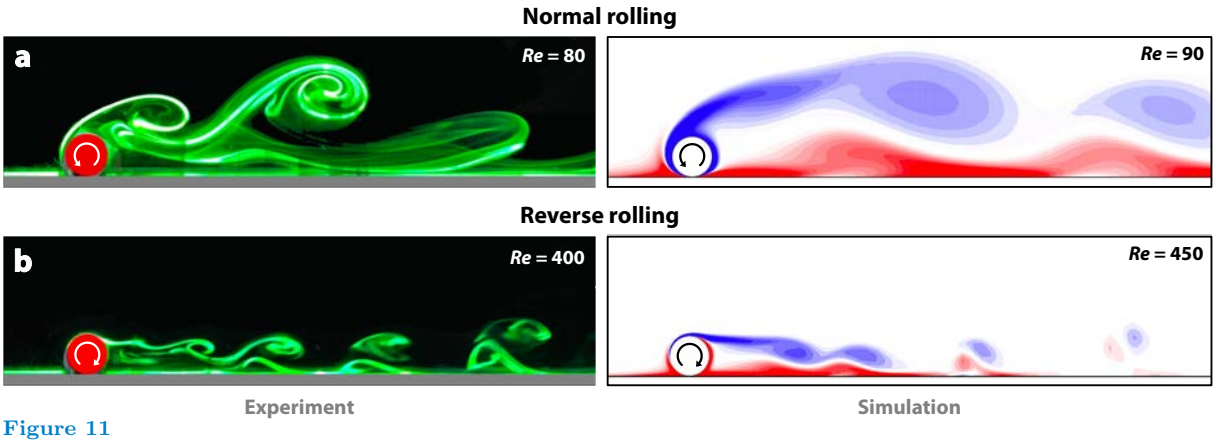

Figure 11

Unsteady two-dimensional wake of a cylinder translating on a wall, for (a) normal rolling ($\alpha = +1$) and (b) reverse rolling ($\alpha = -1$). Left: experimental dye visualizations in a water channel equipped with a moving floor; right: vorticity fields from numerical simulation. Panels a and b adapted with permission from Stewart (2008).

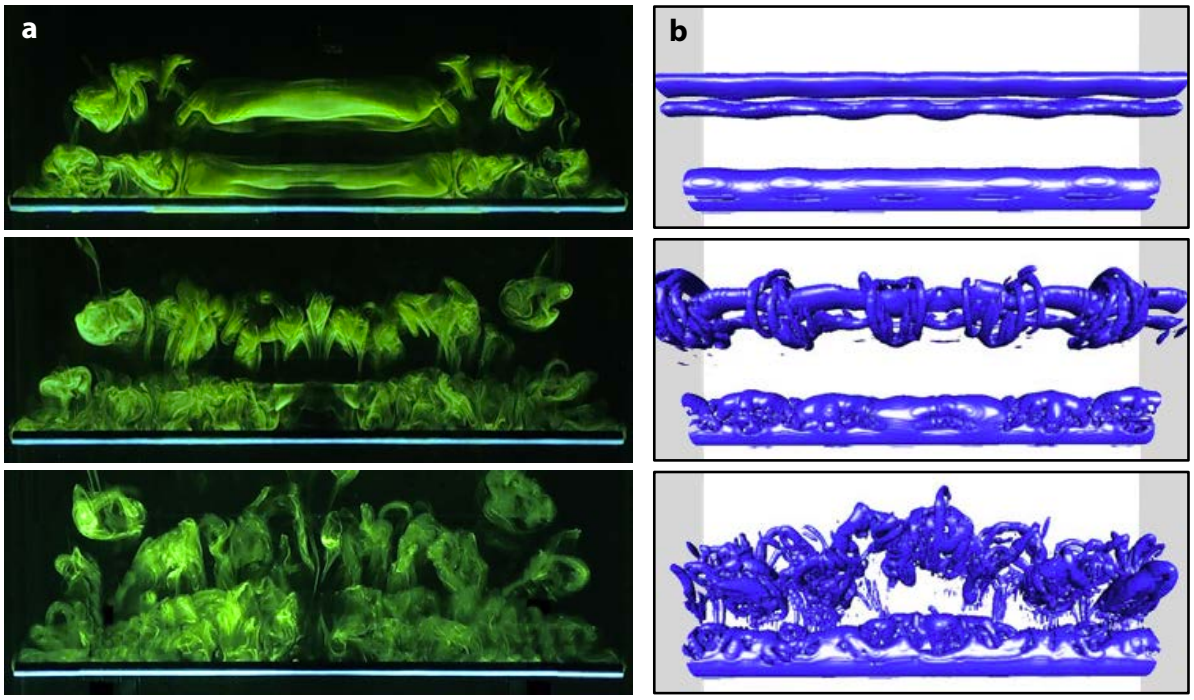

Figure 12

Development of three-dimensionality in the wake of a freely rolling cylinder at $Re = 160$. (a) Experimental dye visualization of the first three shedding cycles after an impulsive start from rest. The cylinder is $47D$ long, with free ends. (b) Isosurface of the *Q-criterion* function (Hunt et al. 1998) from numerical simulation, showing vortical structures during three consecutive shedding cycles after the onset of three-dimensional flow. The cylinder length is $54D$, with periodic boundary conditions. Panel b adapted with permission from Houdroge et al. (2017).

at a smaller angle from the front of the cylinder, so that these vortices advect into the wake further away from the wall. These two effects affect the magnitude of the secondary wall vorticity generated, and so influence the structure and stability of the wake. The details were explored experimentally and numerically by Stewart et al. (2006, 2010b) for cylinders moving at constant speed with a very small fixed gap ($G/D = 0.005$) and for $Re \leq 350$. The transition map as a function of Reynolds number and rotation rate is given in **Figure 10*a***. For a non-rotating (sliding) cylinder, the two-dimensional flow remains steady up to $Re = 165$, beyond which periodic flow is observed, where opposite-signed vortex structures combine and self-propel away from the wall. Linear stability analysis was used to show that the flow becomes three-dimensional directly from steady flow at $Re = 70.5$. This is unlike the situation for an isolated cylinder, where transition to three-dimensional flow occurs from a periodic wake. The transition Reynolds numbers vary with the rotation rate, they increase with decreasing α, and vice versa. Water-tunnel wake visualisations are in good agreement with the numerical simulation predictions, as can be seen, e.g., for the forward- and reverse-rolling cases shown in **Figure 11**. More recently, Houdroge et al. (2017) examined the onset of three-dimensionality of a cylinder rolling *freely* along a wall without slip ($\alpha = 1$), again through experiments and numerical simulation. **Figure 12** shows that wake three-dimensionality can strongly distort wake structures after a few shedding cycles at moderate Reynolds numbers, and additionally that the influence of the free ends of the cylinder propagates rapidly inwards along the span.

4.2. Rolling Spheres

While maintaining some of the flow physics governing rolling-cylinder wakes, there are also some important differences for rolling spheres. In particular, a rolling sphere touches the surface at a single point rather than along a line, which allows the fluid to pass around the sides of the sphere as the gap is reduced. For this reason, wall proximity has a reduced influence in modifying the wake from that of the isolated sphere, compared to the cylinder case. This problem has been explored by Stewart et al. (2008, 2010a) and Rao et al. (2012) for the flow around spheres translating at constant speed and rotating very close to a wall at Reynolds numbers up to several hundred, covering both steady and unsteady regimes. The gap ratio was chosen to be sufficiently small ($G/D = 0.005$), so that the wake flow structures are not sensitive to the gap, even though the lift and drag forces are, as discussed below in section 4.3. The effect of the sign and magnitude of the rotation rate on the wake characteristics up to $Re = 350$ is shown in **Figure 10*b***.

For $\alpha > 0$ (prograde rolling), a compact zone of recirculating fluid is formed and the unsteady flow is marked by the shedding of hairpin vortices analogous to the periodic wake of an isolated sphere. However, for $\alpha < 0$ (retrograde rolling), a streamwise vortex pair appears in the wake, and as Re is increased further the wake undergoes a transition to an antisymmetric mode. A comparison between these two wake states is given in **Figure 13**.

For the forward-rolling sphere with $\alpha = 1$, the wake remains attached and steady at low Reynolds numbers (Stewart et al. 2010a); it is analogous to that of an isolated sphere, i.e., a double-threaded wake consisting of a counter-rotating vortex pair. Transition to unsteady, periodic and symmetric flow occurs at $Re \simeq 139$, as shown through direct numerical simulations by Rao et al. (2012), who also identified a second transition, at $Re \simeq 192$, to unsteady, asymmetrical flow, where the wake exhibits oscillations in the lateral directions. Both transitions were found to be supercritical (non-hysteretic). Visualisations of the symmetric and asymmetric unsteady wakes are shown in **Figure 14**.

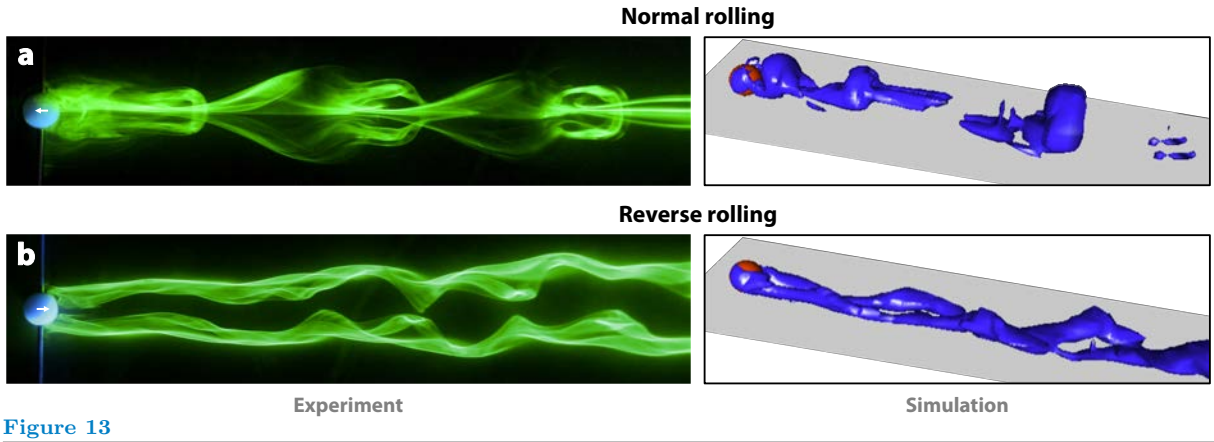

Figure 13

Unsteady wake of a sphere translating on a wall, for (*a*) normal rolling ($\alpha = +1$) and (*b*) reverse rolling ($\alpha = -1$). Left: experimental dye visualizations (top view) at $Re = 200$ in a water channel equipped with a moving floor, reproduced from Stewart et al. (2008), with permission of AIP Publishing. Right: isosurfaces of the λ_2-function (Jeong & Hussain 1995) from numerical simulation, at $Re = 200$ (top) and $Re = 300$ (bottom), showing vortical structures (oblique view), adapted with permission from Stewart et al. (2010a).

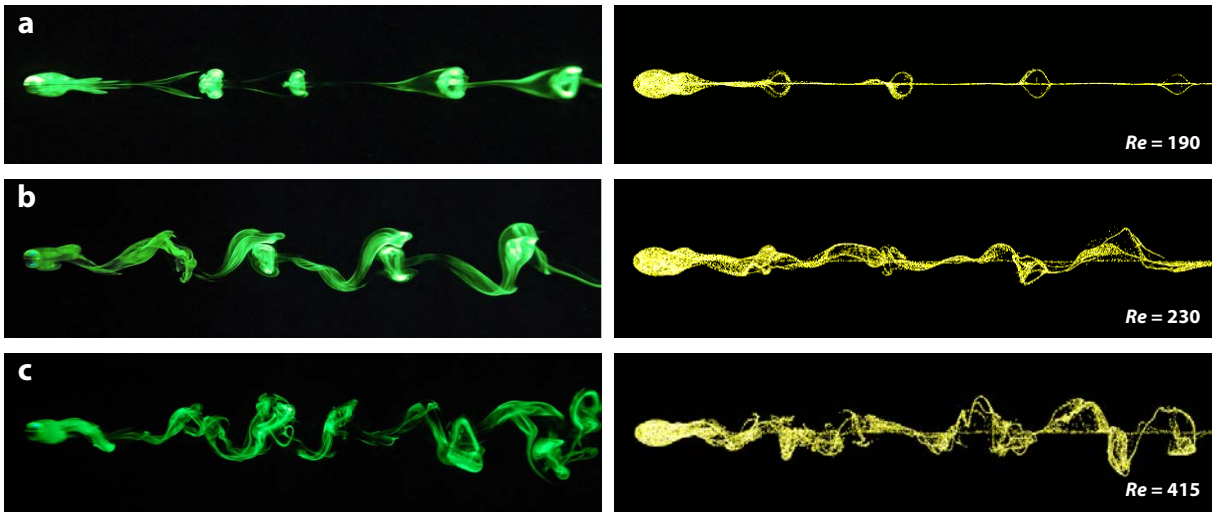

Figure 14

Wake of a sphere rolling in a straight line along a wall at different Reynolds numbers, seen from above. Experimental dye visualization (left) and numerical simulation with tracer particles (right). A bifurcation breaking the initial planar symmetry occurs at $Re = 192$, between panels *a* and *b*. Figure adapted with permission from Rao et al. (2012).

In general, when a body is not forced to move at a constant speed, e.g., in cases where it is rolling down a slope driven by gravity, unsteadiness in its wake leads to oscillations (vibrations) of its trajectory. As well as sphere oscillations in the down-slope direction, there is also considerable movement across the slope. The sidebar, Vortex-Induced Vibrations of Rolling Bodies, gives a few brief details concerning this topic, which is beyond the scope of the present review.

VIV: vortex-induced vibrations, body oscillations caused by time-dependent fluid forces due to vortex shedding

VORTEX-INDUCED VIBRATION OF ROLLING BODIES

Vortex-Induced Vibration (VIV) of rotating bodies is also influenced by the presence of a wall compared to isolated cases (Bourguet & Lo Jacono 2014, Zhao et al. 2018), along with changes to the potential added mass. For a body accelerating in a fluid, the fluid force (drag) resisting this acceleration can be expressed as a mass which is added to the body mass in the equations for the body motion. The added mass coefficient is the ratio of this additional mass to the fluid mass displaced by the body. For a cylinder and a sphere, this coefficient increases from 1 and 1/2, respectively, at infinity, to approximately 2.29 and 0.58, respectively, at the wall for motion parallel to the wall, independent of rotation (Brennen 1982). These increases represent an added resistance to acceleration of the bodies, which should act to mitigate VIV to some extent. However, there are also dramatic changes in the wake structures, for both rolling cylinders (Houdroge et al. 2020a) and rolling spheres (Houdroge et al. 2020b), at least in the low-Reynolds number range. These bodies are found to undergo increasing VIV about their mean rolling speed with decreasing ratio of body and fluid densities, interestingly with spheres having considerably smaller vibration amplitudes than cylinders.

4.2.1. Body forces on rolling spheres. Theoretical analysis has been combined with laboratory experiments to investigate the forces acting on a sphere rolling freely down an incline (Carty 1957, Garde & Sethuraman 1969, Jan & Shen 1995, Verekar & Arakeri 2010, Houdroge et al. 2020b). Under the assumption of a no-slip surface, the sphere reaches a terminal velocity from which an *effective* drag coefficient (C'_D) can be calculated. Note that for a sphere rolling down a slope without slip, this effective C'_D is given by the sum of the standard drag coefficient and the fluid torque coefficient (Houdroge et al. 2020b). The data are presented in the composite plot of **Figure 15*a***. They show that, for low Reynolds numbers, the drag is significantly greater than for a sphere in an unbounded flow (compare with **Figure 9*a***), but it also appears to vary as Re^{-1} up to $Re \approx 100$. Although Carty (1957) and Garde & Sethuraman (1969) followed a similar experimental methodology, drag coefficients calculated in the latter study are up to twice as large as those from the former. Garde & Sethuraman (1969) relate this difference to the longer experimental flume used in their experiments, which leads to more accurate timing and therefore velocity calculations, although their graph is presented with a significant amount of scatter. For $Re \geq 5$, the results of Jan & Shen (1995) are broadly consistent with, although generally well above, the observations of Carty (1957), and their data show considerable scatter, too. It is also unclear why they do not present any values in the range $100 < Re < 1000$.

4.3. The Rolling Paradox

Many careful experimental and numerical studies into the dynamics of rolling/sliding cylinders and spheres in close proximity to a wall have been undertaken. For the numerical studies, in particular, a finite gap was maintained between the cylinder and the wall, due to the problem related to a mesh singularity arising at zero gap, and also to keep a reasonable computational timestep, since the respective timescales governing the gap flow and the global wake dynamics become increasingly separated. For relatively small gaps ($G/D \lesssim 0.01$), vortex formation and shedding is relatively independent of the gap size, but the force coefficients are strongly affected, as shown by the examples in **Figure 16** (see also **Figure 9**).

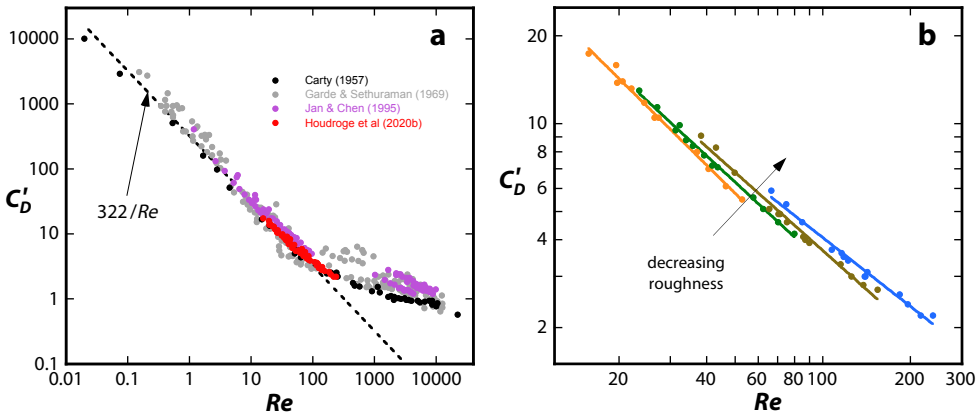

Figure 15

Mean effective drag coefficient (including torque) of a sphere rolling down an incline, as function of Reynolds number. (*a*) Collection of various experimental data. (*b*) Close-up of the measurements by Houdroge et al. (2020b), showing an increase of the drag with decreasing relative surface roughness (increasing diameter) of the sphere.

The so-called rolling paradox arises from theoretical/analytical results concerning the flow in the gap region using lubrication theory. Application of this theory to the rolling cylinder and rolling sphere problems can be found, e.g., in Merlen & Frankiewicz (2011) and Goldman et al. (1967), respectively. They predict that, as the gap size approaches zero, the drag force on the body diverges as $(D/G)^{1/2}$ for the cylinder, and as $\ln(D/G)$ for the sphere, for any combination of sliding and rolling, due to the generation of a pressure peak diverging to positive infinity in front of the body, and another peak diverging to negative infinity behind it. This implies that a cylinder or sphere in contact with a solid surface would be impossible to move along this surface, which is contrary to common observation, and that any rolling or sliding motion along the wall would involve a liquid film of finite thickness between the two, i.e., the absence of solid-to-solid contact. Goldman et al. (1967) calculated that the gap size compatible with the drag coefficients of a rolling sphere determined experimentally by Carty (1957) (**Figure 15a**) would be of the order of atomic dimensions, which is well outside the validity domain of the theory. Goldman et al. (1967) put forth six points of discussion in an attempt to explain the discrepancy between the idealised model provided by lubrication theory and experimental data. They include the roughness of the sphere and/or wall, compressibility effects and cavitation linked to the large positive and negative pressures encountered, breakdown of the continuity assumption at very small gaps, inertial and non-Newtonian effects, and deformations of the sphere by the high pressure gradient.

Surface roughness was dismissed by Goldman et al. (1967), since Carty's (1957) drag data apparently did not show differences between the various spheres of different roughnesses used. Revisiting the data (**Figure 16**), it appears that this conclusion is not clearly justified. Specifically, the data points are not frequent enough to allow differentiation, and the results are presented on a log-log plot that masks any such trends. (On such a log-log plot with sparse points, a variation in drag coefficient of 100% is essentially not discernible!). More recent experiments by Houdroge et al. (2020b) appear to show that different relative surface roughnesses do in fact lead to different drag coefficient variations with macroscopic Reynolds

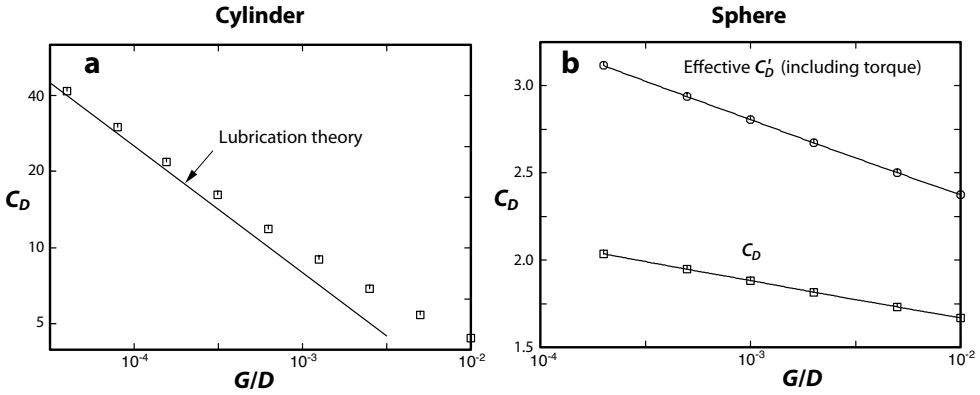

Figure 16

Drag coefficient for rolling bodies as function of gap size from direct simulation. (*a*) Cylinder at $Re = 50$. The line shows the prediction from lubrication theory: $C_D = 4\pi/[Re(G/D)^{1/2}]$. Panel *a* adapted with permission from Houdroge et al. (2020a). (*b*) Sphere at $Re = 100$. The lines represent scalings in line with lubrication theory: $C_D \sim \ln(D/G)$.

number, as seen in **Figure 15*b***. By providing an effective average gap, the roughness of the body (and/or the wall) therefore appears to be a determining factor for its motion along a wall. Interestingly, the drag prediction from direct numerical simulation for smooth rolling spheres at higher Reynolds number (**Figure 16*b***) appears to approach the experimentally observed values given by Carty (1957) and Houdroge et al. (2020b) (**Figure 15**), as the gap ratio approaches expected relative roughness ratios ($\delta/D \sim 10^{-6}$–10^{-7}, where δ is the mean asperity height).

Roughness effects were further investigated by Smart et al. (1993), who extended the work of Goldman et al. (1967) by proposing that roughness elements can in fact lead to physical contact with the plane when the separation distance between the surfaces is of the order of the roughness height, and that the plane will then exert a nonhydrodynamic force and torque on the sphere. Their research gave quantitative agreement between measured translational and rotational velocities and their theory for small inclination angles of the plane, however their data at high angles showed a greater discrepancy, in line with a larger apparent gap than the one considered. King & Leighton (1997), Galvin et al. (2001) and Zhao et al. (2002) argued that rather than experiencing a single surface roughness and separation distance, the sphere has two scales of roughness: small bumps that support the particle at rest and at low angles, and larger roughness elements distributed sparsely on the surface that dominate the separation at higher angles. Galvin et al. (2001) and Zhao et al. (2002) developed a theoretical model of this phenomena and tested it experimentally, confirming that at low angles, the sphere is in contact with the wall via the small asperities, whereas at high angles the large asperities may cause the sphere to lift off the wall and move without continuous contact.

Although a smooth bump, no matter the radius, will induce an unlimited pressure force as the gap between it and a smooth surface decreases, a roughness element or asperity of small enough dimension can decrease the gap to molecular dimension, whereby contact can be said to occur (Smart & Leighton 1989, Lecoq et al. 2004). The observation that in practice contact does occur is therefore a consequence of physical considerations outside the

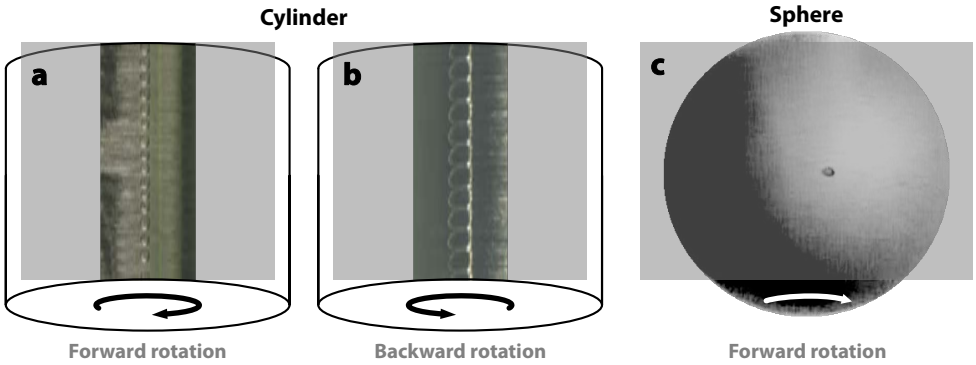

Figure 17

Experimental visualization of cavitation bubbles in the gap region of bluff bodies moving along a wall in a Stokes flow. Views from below through the transparent wall. All bodies move to the left. (*a*) Cylinder in forward rotation, $Re = 1.2$, $\alpha \approx 1$. (*b*) Cylinder in backward rotation, $Re = 2.9$, $\alpha \approx -0.2$. Panels *a* and *b* adapted from Seddon & Mullin (2006), with permission of AIP Publishing. (*c*) Sphere in forward rotation, $Re = 0.5$, $\alpha \approx 0.3$. Panel *c* adapted with permission from Ashmore et al. (2005), copyright 2005 by the American Physical Society.

assumptions of surface smoothness, fluid continuum and incompressibility, such as roughness closing the gap to the order of the fluid molecular dimension, or ultimately other short-range interactions like van der Waals forces. The precise details of how solid-to-solid contact occurs, which are essential for an understanding of the resistive forces due to contact, the effective hydrodynamic gap, and the rolling speed of bluff bodies, are presently still not entirely clear.

When the body is surrounded by a liquid, cavitation can occur for small gaps, when the diverging negative pressure decreases below the vapour pressure, an effect already investigated by Taylor (1963) for lubrication flow. Merlen & Frankiewicz (2011) and Prokunin (2003) have analysed the cases of cylinders and spheres rolling along a plane wall. When cavitation appears, it eliminates the large negative pressure peak behind the body, but not the positive peak ahead of it. This asymmetry results in a net lift force, which can push the body further away from the surface, while at the same time maintaining a large drag force. (Similarly, fluid compressibility modifies the pressure distribution near contact but infinite pressures still arise from zero gap.) Experiments by Seddon & Mullin (2006) on cylinders moving close to a wall in a highly viscous liquid have shown that cavitation appears in the gap region in the form of a periodic array of vapour bubbles (**Figure 17*a***), whereas Prokunin (2004) and Ashmore et al. (2005) visualised a single cavitation bubble for the case of a rolling sphere (**Figure 17*b***).

5. BLUFF BODIES IMPACTING ON A WALL

In this section, we are chiefly concerned with the flow structures arising from a rigid body impacting on a rigid wall, and not the elastic and/or plastic deformations that may occur in the solid structures (for the latter, see, e.g., Yildirim et al. 2017). In this case, the initial stage of the wake evolution is clearly related to those of impulsively arrested bodies discussed in section 2.3. In addition, in a broader sense, the later wake evolution involves secondary

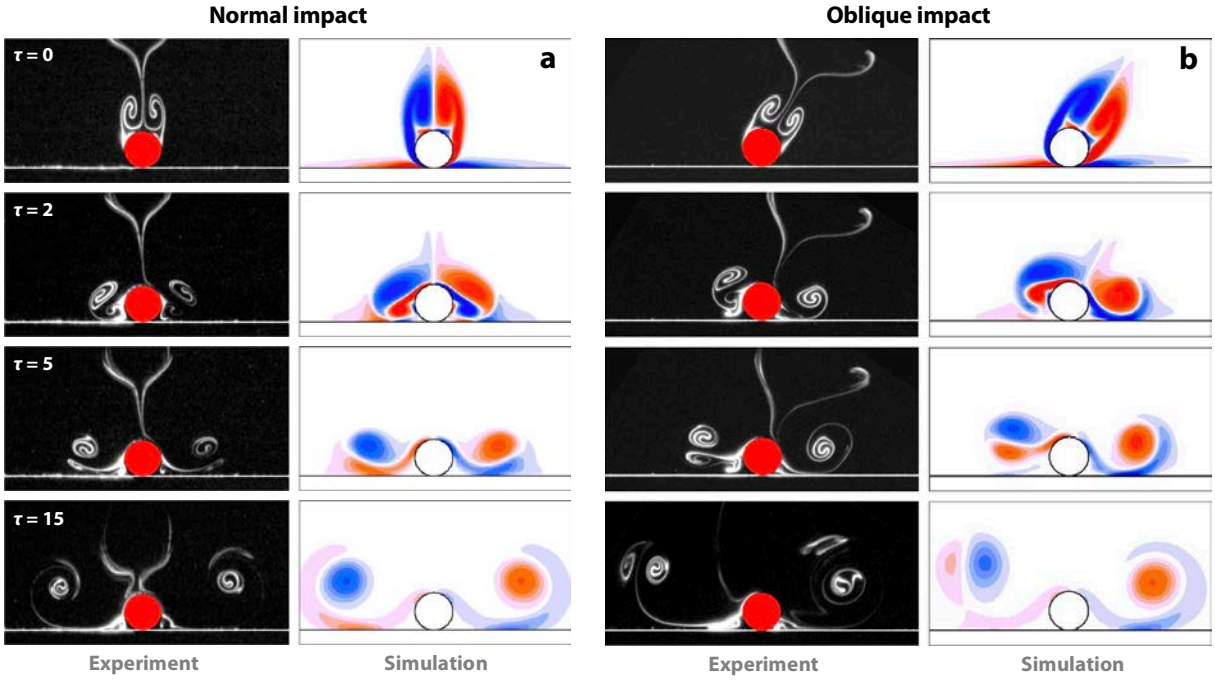

Figure 18

Flow generated by the impact of a circular cylinder on a solid wall at $Re = 200$ for $L/D = 4$. Experimental dye visualization and numerical vorticity fields. (*a*) Normal impact, and (*b*) oblique impact at $\theta = 57°$. Non-dimensional time $\tau = tU/D$ is counted from the moment of impact. Panels *a* and *b* reprinted from Leweke et al. (2008), with permission from Elsevier.

vorticity generation from the proximity of primary vortices to the wall that subsequently leads to vortex pair formation and self-propulsion away from the body, showing similarities with the wake evolution of rolling or sliding bodies in section 4.

5.1. Impacting Cylinders

Leweke et al. (2008) presented results from experiments and simulations on the flow around a circular cylinder on impact with a solid wall. At low Reynolds numbers, when impacting normally to the wall, the attached counter-rotating vortices that form during the pre-impact motion of the cylinder, overtake it on impact, one on each side, and then initially move outwards along the wall, due to the influence of their image vortices. Subsequently, they experience a weak rebound associated with secondary vorticity generated at both the cylinder and wall (**Figure 18*a***). For higher Reynolds numbers, the secondary vorticity generated rolls up into discrete secondary vortices, which orbit the primary vortices and undergo a three-dimensional elliptic instability (**Figure 20*a***), a phenomenon known to occur in strained vortical flows (Kerswell 2002). Beyond a Reynolds number of a few hundred, this process leads to breakdown of the vortex system into small-scale structures. This flow behaviour is similar to the case of a counter-rotating vortex pair impinging on a solid wall (Leweke et al. 2016).

Image vortex: virtual vortex located symmetrically with respect to a surface, having the same effect as the boundary condition of zero normal velocity at this surface

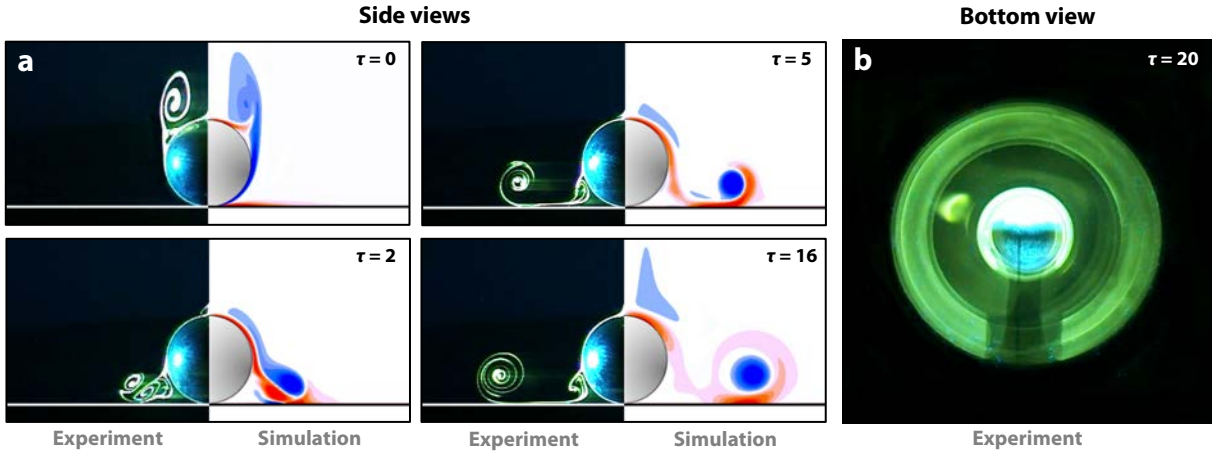

Figure 19

Sphere impact at $Re = 800$ for $L/D = 5$. (*a*) Side views with experimental dye visualizations and numerical vorticity fields. Panel *a* adapted from Leweke et al. (2004a), with permission of AIP Publishing. (*b*) Bottom view, experimental dye visualization. Panel *b* reprinted from Leweke et al. (2004b), with permission of AIP Publishing.

Oblique cylinder impacts have also been examined (**Figure 18*b***). Not surprisingly, this asymmetry leads to different flows generated on each side of the cylinder. The vortical structures that develop on the side beneath the cylinder path appear similar to those for the normal impact case, while generation of secondary vorticity at the wall on the opposite side decreases with growing impact angle, leading to changes in the pair formation process. For higher impact angles, the source of secondary vorticity generation is mostly restricted to the cylinder surface, resulting in the formation of a vortex dipole which, through self-induction, leads to rebound and self advection of the primary vortex to greater heights than occurs for the normal impact.

5.2. Impacting Spheres

The flow generated by the normal impact of a sphere on a wall bears similarities with the cylinder case. The recirculation zone behind the moving sphere takes here the form of a vortex ring. On impact, this ring overtakes the sphere, leading again to the generation of secondary vorticity at the sphere surface and at the wall, which separates and wraps around the primary ring (**Figure 19**). At low Reynolds numbers, the flow remains axisymmetric at all times, whereas for $Re \gtrsim 1000$ an instability develops in the azimuthal direction of the primary vortex ring, as seen in **Figure 20*b***. Leweke et al. (2006) endeavoured to gain an understanding of the flow physics involved in this instability. They found that the flow structures that developed were consistent with a centrifugal instability of the primary vortex ring core surrounded by secondary vorticity of opposite sign drawn up from the wall. Both the growth rate and azimuthal mode numbers, predicted from idealized centrifugal instability theory based on the local velocity profile, show good agreement with those observed in the experiments, simulations and linear stability analysis of the frozen flow state. Since the cross section of the primary ring becomes elliptical after the impact, the stability of the ring was also tested against elliptic instability. Although the predicted azimuthal mode numbers matched well, the predicted growth rates were negative.

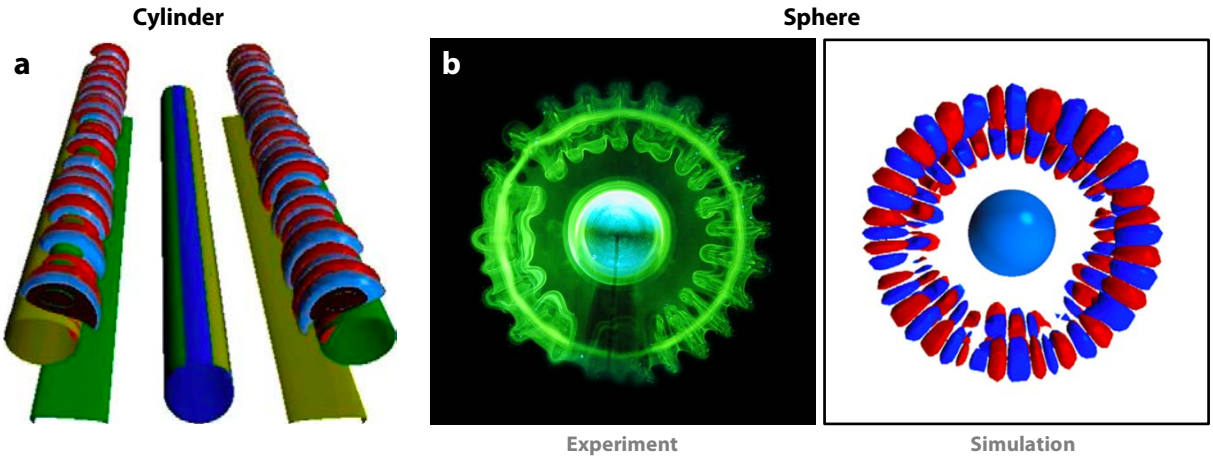

Figure 20

Three-dimensional instability of the flow generated by a wall impact. (*a*) Cylinder at $Re = 400$ for $L/D = 5$. Isosurfaces of vorticity from numerical simulation, showing an elliptic instability of the secondary vortex. Panel *a* reproduced from Thompson et al. (2006a), with permission from Elsevier. (*b*) Sphere for $L/D = 5$. Dye visualization in water at $Re = 1500$ (left) and isocontours of radial vorticity from simulation at $Re = 1200$ (right), showing the centrifugal instability of the primary vortex. Panel *b* reprinted from Leweke et al. (2004a), with permission of AIP Publishing.

The dynamics bear resemblance to the related case of a vortex ring impacting on a wall, studied by Lim (1989), Lim et al. (1991), Masuda et al. (2012), Orlandi & Verzicco (1993), Swearingen et al. (2000) and Walker et al. (1987). In both configurations, the primary vortex ring draws up secondary vorticity generated as it nears the wall, and then the ring structure expands radially, leading to qualitatively similar vorticity patterns. However, the isolated impacting ring becomes unstable through fragmentation of the secondary vorticity into quasi-discrete vortices when the Reynolds number is sufficiently large. This secondary vortex fragmentation has a relatively low azimuthal wavenumber (∼6 waves along the ring perimeter, compared to ∼20 for the sphere impact in **Figure 20*b***), and involves self- and mutual induction from the primary vortex, as discussed in the above articles. Of interest, direct simulations of vortex ring impact indicate that this fragmentation process arrests relatively quickly, and subsequently a shorter-wavelength instability manifests, possibly attributable to the same centrifugal mechanism causing ring breakup for the sphere impact.

A comparison between circular cylinder impact and normal sphere impact have revealed important differences in the developed wakes. The vortex stretching of the primary vortex as the ring expands radially is not present for the cylinder impact, and this leads to a reduction in core size and accelerated vorticity cross-diffusion in the axisymmetric geometry. These effects delay the onset of three-dimensional instabilities in the vortical flows generated on impact of a spherical particle with a wall, in comparison to the two-dimensional counterpart.

Comparing with the flow generated by a body arrested in isolation (section 2.3), the presence of the wall has two main effects: it restricts and modifies the trajectories of the primary vortices, through induction from the image vortices representing the boundary condition of vanishing normal velocity, and it is a further source of secondary vorticity. Together, these effects can produce vortex configurations not found for freely arresting bodies, e.g., where the secondary vorticity wraps around the primary vortex in a band

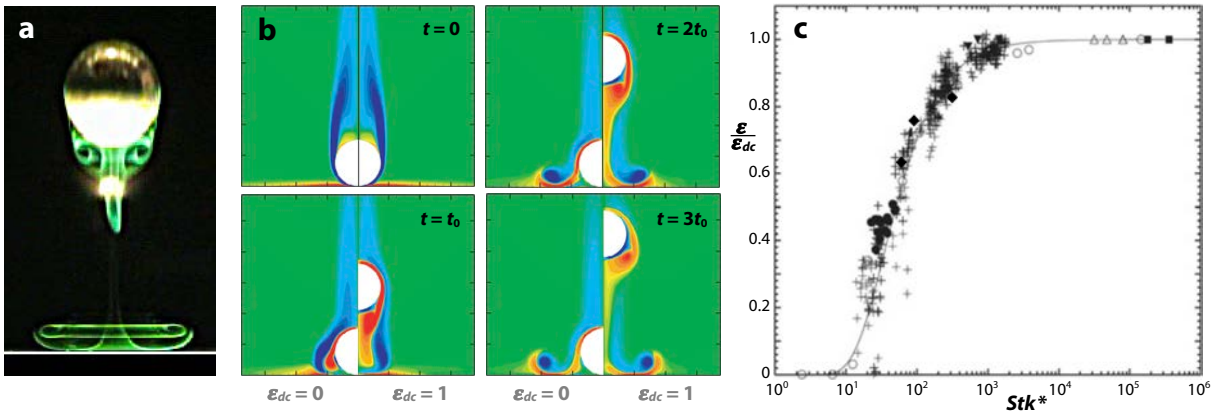

Figure 21

Rebound of a sphere from a wall. (*a*) Forced rebound for $L/D = 5$, $Re = 800$ and $\varepsilon_{dc} = 1$. Dye visualization in water. Panel *a* reprinted with permission from Thompson et al. (2007). (*b*) Rebound after a free fall under gravity for $L/D = 5$, $Re = 865$ (at impact). Vorticity contours from numerical simulations, comparing the cases of plastic ($\varepsilon_{dc} = 0$, left half of the images) and elastic ($\varepsilon_{dc} = 1$, right half) collisions. $t_0 = 0.8\sqrt{D/g}$ (g: gravitational acceleration). (*c*) Normalized coefficient of restitution as function of modified Stokes number, collected from various studies. Panels b and c adapted with permission from Ardekani & Rangel (2008).

(**Figures 18*a*** and **19*a***) instead of forming a discrete concentrated vortex (**Figure 5**), which can lead to different types of three-dimensional instability (centrifugal instability) at higher Reynolds numbers.

5.3. Rebounding Bluff Bodies

The configuration involving a spherical particle in a viscous fluid rebounding from a solid surface after a normal collision has been investigated in numerous studies including analytical/numerical work by Davis et al. (1986), Lian et al. (1996), Ardekani & Rangel (2008), Li et al. (2012) and Brändle de Motta et al. (2013), as well as experiments by Joseph et al. (2001), Gondret et al. (1999, 2002) and Ruiz-Angulo & Hunt (2010). Most of these studies focused on the flow structure around the point and near the time of impact, and on the determination of the coefficient of restitution (ε), given by the ratio of rebound velocity to particle impact velocity. Few studies have considered the vortical structures in a more extended region and time interval around the collision. The visualization by Thompson et al. (2007) and simulations by Ardekani & Rangel (2008) show that the primary vortex ring in the wake of the approaching sphere is left behind after the rebound and exhibits dynamics similar to that for a sphere with no rebound – compare **Figures 19** and **21*a,b***.

The coefficient of restitution was found to depend on the non-dimensional Stokes number $Stk = (1/9)(\rho_p/\rho_f)Re$, where ρ_p and ρ_f are the particle and fluid densities, respectively, and Re is the particle Reynolds number at impact, with only a weak dependence on the elastic properties of the material (Joseph et al. 2001). This parameter compares particle inertia to viscous effects; according to Legendre et al. (2005) the effect of added mass should also be included: $Stk^* = (1/9)(\rho_p/\rho_f + C_m)Re$, with C_m the added mass coefficient. No rebound is found to occur below a critical value of $Stk^* \approx 10$, and the coefficient of restitution approaches that for a dry collision (ε_{dc}) for $Stk^* \gtrsim 1000$, as shown in **Figure 21*c***.

As for rolling bodies discussed in sections 4.2.1 and 4.3 above, the issue of whether there is solid-to-solid contact, or if lubrication forces prevent this contact, is relevant also to a bluff-body impact and rebound. In the study by Davis et al. (1986), the pressure forces in the viscous liquid lubrication film between the particle and the wall during the collision were found to be sufficiently large to cause the particles to deform elastically and rebound. The Stokes number dependence has been attributed to the drainage of the lubrication film. In this model of elastohydrodynamic collisions based on lubrication theory, the two solids never touch.

Effects that lead to a breakdown of the lubrication approach include again surface roughness (Smart & Leighton 1989). Davis (1987) already suggested that when the gap between the surfaces becomes equal to the size of the largest surface roughness element, solid-to-solid contact of the roughness bumps could occur due to discrete molecular nature of the fluid and/or attractive London-van der Waals forces. More recently, Birwa et al. (2018) have studied the collision between spheres and a wall in a viscous fluid, focusing on the question of solid-to-solid contact. For Stokes numbers below the rebound threshold, the lubrication film forces were found to decelerate the spheres to zero velocity before reaching the wall. As soon as rebound occurred for increasing Stokes numbers, contact between the two solids was systematically detected. The explanation provided was that the lubrication film thickness needed to produce the force for stopping the sphere motion is significantly smaller than the roughness of the particle or the wall, and therefore contact is made via the roughness elements.

INTERACTION WITH A FREE SURFACE

There are many important interactions that take place at free, or nearly free, surfaces, such as for oceans, lakes and rivers, as well as industrial processes involving risers, bridge piers, mixing vessels and bioreactors. A number of studies have provided valuable insights into the surprising wake structures and free-surface response for non-rotating submerged or semi-submerged cylinders or spheres (Sheridan et al. 1997, Reichl et al. 2003, 2005, Kawamura et al. 2002, Chaplin & Teigen 2003, Koo et al. 2004, Shao et al. 2013, Vlachos & Tellionis 2008, Sareen et al. 2018). Far from being a passive boundary, the free surface, when distorted, becomes a rich source of vorticity that can remarkably change the wake of a bluff body (Brøns et al. 2014, Terrington et al. 2020). However, the effects of the interface on the force distribution on the body, vortex generation and turbulence structures, and air-water interface structures, still require much further study.

6. CONCLUDING REMARKS

In this review, we discuss the effect of a wall on the wake structures and transitions of bluff bodies moving relative to the wall. The review is restricted to the generic two- and three-dimensional bluff bodies – the circular cylinder and the sphere, respectively – and to the ambient fluid being at rest relative to the wall. This excludes the class of flows for which boundary layers form due to the fluid flow along the wall and where the bluff body is fixed to the wall, such as is typical in wind engineering applications. The simplified flow allows a clearer analysis of the direct effect that the wall itself has on the wakes. We also consider only interactions with a rigid wall; the sidebar, Interaction with a Free Surface, briefly addresses the configuration of bluff bodies placed near a fluid-fluid interface.

SUMMARY POINTS

1. Proximity to a wall changes the bluff-body wake structures and transitions significantly. For example, the strong absolute instability causing Bénard-von Kármán vortex shedding for an isolated cylinder becomes much weaker in the immediate presence of a wall, with a predominately single-sided wake, and a steady three-dimensional transition mode appears at higher Reynolds numbers.
2. Flow underneath a cylinder or sphere is restricted as the body is moved closer to the wall, which effectively eliminates shedding of near-wall vortices. However, the proximity of the upper shed vortices to the wall leads to secondary vorticity generation there, which can roll up into discrete structures forming pairs with the upper vortex. These pairs propagate away from the wall, causing a significant spread of the wake. This mechanism dominates the flow dynamics for the cylinder case, but is less important for a sphere.
3. For small gaps (less than 1% of the body diameter), the gap flow effectively becomes uncoupled from the global flow around rolling bodies, hence simulation of rolling bodies with small imposed gaps produce wake dynamics relatively insensitive to the gap ratio. However, this is not true for the lift and especially the drag force, which are very sensitive to gap size.
4. The flow dynamics for bluff bodies impacting a surface is governed by the starting distance and the Reynolds number. A vortex system is formed from the initial wake (vortex pair for the cylinder, vortex ring for the sphere) and secondary wall vorticity, which propagates away from the impact point. At higher Reynolds number, it becomes three-dimensionally unstable, through an elliptic instability in the case of a cylinder, and a centrifugal-type instability for the sphere.
5. For freely rolling or sliding bodies, surface roughness appears to be a key element, leading to an effective contact between the two solids, while at the same time providing an effective finite gap. Predicted drag coefficients for smooth spheres rolling without slip are similar to those observed in experiments for a roughness height of the order of the chosen gap size. However, this requires further investigation.

FUTURE ISSUES

1. Studies of the wakes of sliding and rolling bodies of other geometries (elliptical cylinders, cubes) and the combined wakes of multiple bodies, particularly spheres, in motion near walls will extend current knowledge to a broader set of applications.
2. Simulations of rolling/sliding bodies near surfaces at higher Reynolds numbers are required to examine turbulent transition and fully turbulent wakes.
3. The effects of body rotation, as well as wall and body material elasticity, on the wakes of impacting bluff bodies are largely unexplored.
4. The details of the physics of solid-to-solid contact due to surface roughness need to be further addressed, ideally through a combination of careful experiments, detailed numerical simulations resolving the flow near the gap, and theoretical analysis.
5. How bluff bodies interact with free surfaces and multi-fluid interfaces is yet to be investigated in detail.

DISCLOSURE STATEMENT

The authors are not aware of any biases that might be perceived as affecting the objectivity of this review.

ACKNOWLEDGMENTS

We wish to acknowledge generous support from the Australian Research Council through Discovery Project grants: DP130100822, DP150102879 & DP200100794. MCT and KH also acknowledge generous computing allocations from the National Computing Infrastructure (Canberra) and Pawsey Supercomputing Centre (Perth) through grants n67 & d71.

LITERATURE CITED

Ardekani AM, Rangel H. 2008. Numerical investigation of particle-particle and particle-wall collisions in a viscous fluid. *J. Fluid Mech.* 596:437–66

Ashmore J, del Pino C, Mullin T. 2005. Cavitation in a lubrication flow between a moving sphere and a boundary. *Phys. Rev. Lett.* 94:124501

Barkley D, Henderson RD. 1996. Three-dimensional Floquet stability analysis of the wake of a circular cylinder. *J. Fluid Mech.* 322:215–41

Bearman PW. 1984. Vortex shedding from oscillating bluff bodies. *Annu. Rev. Fluid Mech.* 16:195–222

Berger E, Wille R. 1972. Periodic flow phenomena. *Annu. Rev. Fluid Mech.* 4:313–40

Birwa SK, Rajalakshmi G, Govindarajan R. 2018. Solid-on-solid contact in a sphere-wall collision in a viscous fluid. *Phys. Rev. Fluids* 3:004302

Bourguet R, Lo Jacono D. 2014. Flow-induced vibrations of a rotating cylinder. *J. Fluid Mech.* 740:342–80

Brändle de Motta JC, Breugem W-P, Gazanion B, Estivalezes J-L, Vincent S, Climent E. 2013. Numerical modelling of finite-size particle collisions in a viscous fluid. *Phys. Fluids* 25:083302

Brennen CE. 1982. *A review of added mass and fluid inertial forces*. Tech. Rep. N62583-81-MR-554, Naval Civil Eng. Lab., Port Hueneme, CA

Brenner H. 1961. The slow motion of a sphere through a viscous fluid towards a plane surface. *Chem. Eng. Sci.* 16:242–51

Brøns M, Thompson MC, Leweke T, Hourigan K. 2014. Vorticity generation and conservation for two-dimensional interfaces and boundaries. *J. Fluid Mech.* 758:63–93

Brücker C. 2001. Spatio-temporal reconstruction of vortex dynamics in axisymmetric wakes. *J. Fluids Struct.* 5:543–54

Carty JJ. 1957. *Resistance coefficients for spheres on a plane boundary*. BSc Thesis, MIT.

Chaplin JR, Teigen P. 2003. Steady flow past a vertical surface-piercing circular cylinders. *J. Fluids Struct.* 18:271–85

Cherukat P, McLaughlin JB. 1994. The inertial lift on a rigid sphere in a linear shear flow field near a flat wall. *J. Fluid Mech.* 263:1–18

Chomaz JM, Bonneton P, Hopfinger EJ. 1993. The structure of the near wake of a sphere moving horizontally in a stratified fluid. *J. Fluid Mech.* 254:1–21

Choi H, Jeon W-P, Kim J. 2008. Control of flow over a bluff body. *Annu. Rev. Fluid Mech.* 40:113–9

Clark HM. 1992. The influence of the flow field in slurry erosion. *Wear* 152:223–40

Davis RH. 1987. Elastohydrodynamic collisions of particles. *PCH Physicochem. Hydrodyn.* 9:41–52

Davis RH, Serayssol JM, Hinch EJ. 1986. The elastohydrodynamic collision of two spheres. *J. Fluid Mech.* 163:479–97

Dobson J, Ooi A, Poon EKW. 2014. The flow structures of a transversely rotating sphere at high rotation rates. *Comput. Fluids* 102:170–81

Elastohydrodynamic modelling of sphere rebound.

Dušek J. Le Gal, P. & Fraunié 1994. A numerical and theoretical study of the first Hopf bifurcation in a cylinder wake. *J. Fluids Mech.* 264: 59–80

Eames I, Dalziel SB. 1999. Resuspension by an impacting sphere. *Phys. Fluids* 11:S11

Ern P, Risso F, Fabre D, Magnaudet J. 2012. Wake-induced oscillatory paths of bodies freely rising or falling in fluids. *Annu. Rev. Fluid Mech.* 44:97–121

Galilei G. 1638. *Dialogues Concerning Two New Sciences*. Transl. H Crew, A de Salvio, 1914. New York: Macmillan (From Italian and Latin)

Galvin KP, Zhao Y, Davis RH. 2001. Time-averaged hydrodynamic roughness of a non-colloidal sphere in low Reynolds number motion down an inclined plane. *Phys. Fluids A* 13:3108–9

Garde RJ, Sethuraman S. 1969. Vorticity generation and wake transition for a translating circular cylinder: Wall proximity and rotation effects. *Houille Blanche* 7:727–32

Ghidersa B, Dušek J. 2000. Breaking of axisymmetry and onset of unsteadiness in the wake of a sphere. *J. Fluid Mech.* 423: 33–69

Giacobello M, Ooi A, Balachandar S. 2009. Wake structure of a transversely rotating sphere at moderate Reynolds numbers. *J. Fluid Mech.* 621:103–30

Goldman AJ, Cox RG, Brenner H. 1967. Slow viscous motion of a sphere parallel to a plane wall—I Motion through a quiescent fluid. *Chem. Eng. Sci.* 22:637–51

Gondret P, Hallouin E, Lance M, Petit L. 1999. Experiments on the motion of a solid sphere toward a wall: From viscous dissipation to elasto-hydrodynamic bouncing. *Phys. Fluids* 11:2803–5

Gondret P, Lance M, Petit L. 2002. Bouncing motion of spherical particles in fluids. *Phys. Fluids* 14:643–52

He W, Gioria R, Pérez J, Theofilis V. 2017. Linear instability of low Reynolds number massively separated flow around three NACA airfoils. *J. Fluid Mech.* 811:701–41

Henderson RD. 1997. Nonlinear dynamics and pattern formation in turbulent wake transition. *J. Fluid Mech.* 353:65–112

Homer. 9th-8th century BC. *The Odyssey*, book 11, lines 593–600. Transl. AT Murray, 1919. Cambridge, MA: Harvard Univ. Press (From Greek)

Houdroge FY, Leweke T, Hourigan K, Thompson MC. 2017. Two- and three-dimensional wake transitions of an impulsively started uniformly rolling circular cylinder. *J. Fluid Mech.* 826:32–59

Houdroge FY, Leweke T, Hourigan K, Thompson MC. 2020a. Wake dynamics and flow-induced vibration of a freely rolling cylinder. *J. Fluid Mech.* (submitted)

Houdroge FY, Zhao J, Leweke T, Hourigan K, Thompson MC. 2020b. Dynamics and fluid-structure interactions of spheres rolling down an inclined plane. *J. Fluid Mech.* (in preparation)

Huang WX, Sung HJ. 2007. Vortex shedding from a circular cylinder near a moving wall. *J. Fluids Struct.* 23:1064–76.

Hunt JCR, Wray AA, Moin P. 1998. Eddies, streams, and convergence zones in turbulent flows. In *Proceedings of the 1988 Summer Program*, pp. 193–208. Center for Turbulence Research, Stanford Univ., Stanford, CA

Jan C-D, Shen H-W. 1995. Drag coefficients for a sphere rolling down an inclined channel. *J. Chin. Inst. Eng.* 18:493–507

Jeong J, Hussain F. 1995. On the identification of a vortex. *J. Fluid Mech.* 285:69–94

Johnson TA, Patel, VC. 1999. Flow past a sphere up to a Reynolds number of 300. *J. Fluid Mech.* 378:19–70

Joseph GG, Zenit R, Hunt ML, Rosenwinkel AM. 2001. Particle-wall collisions in a viscous fluid. *J. Fluid Mech.* 433:329–46

Kawamura T, Mayer S, Garapon A, Sorensen L. 2002. Large eddy simulation of a flow past free surface piercing circular cylinder. *ASME J. Fluids Engg* 124:91–101

Kerswell RR. 2002. Elliptical instability. *Annu. Rev. Fluid Mech.* 34:83–113

Kim D. 2009. Laminar flow past a sphere rotating in the transverse direction. *J. Mech. Sci. Technol.* 23:578–89

King MR, Leighton Jr DT. 1997. Measurement of the inertial lift on a moving sphere in contact

Lubrication theory for a sphere moving along a wall.

with a plane wall in a shear flow. *Phys. Fluids* 9:1248–55
Koo B, Yang J, Yeon SM, Stern F. 2004. Reynolds and Froude number effect on the flow past an interface-piercing circular cylinder. *Int. J. Nav. Archit. Ocean Eng.* 6:529–61
Lecoq N, Anthore R, Cichocki K, Szymczak P, Feuillebois F. 2004. Drag force on a sphere moving towards a corrugated wall. *J. Fluid Mech.* 513:247–64
Legendre D, Daniel C, Guiraud P. 2005. Experimental study of a drop bouncing on a wall in a liquid. *Phys. Fluids* 17:1–13.
Leweke T, Le Dizès S, Williamson CHK. 2016. Dynamics and instabilities of vortex pairs. *Annu. Rev. Fluid Mech.* 48:507-41
Leweke T, Thompson MC, Hourigan K. 2004a. Vortex dynamics associated with the collision of a sphere with a wall. *Phys. Fluids* 16:L74-7
Leweke T, Thompson MC, Hourigan K. 2004b. Touchdown of a sphere. *Phys. Fluids* 16:S5
Leweke T, Thompson MC, Hourigan K. 2006. Instability of the flow around an impacting sphere. *J. Fluids Struct.* 22:961–971
Leweke T., Schouveiler L, Thompson MC, Hourigan K. 2008. Unsteady flow around impacting bluff bodies. *J. Fluids Struct.* 24:1194–203
Li X, Hunt ML, Colonius T. 2012. A contact model for normal immersed collisions between a particle and a wall. *J. Fluid Mech.* 691:123–45
Lian G, Adams MJ, Thornton C. 1996. Elastohydrodynamic collisions of solid spheres. *J. Fluid Mech.* 311:141–52
Lim TT. 1989. An experimental study of a vortex ring interacting with an inclined wall. *Exp. Fluids* 7:453–63
Lim TT, Nichols TB, Chong MS. 1991. A note on the cause of the rebound in the head-on collision of a vortex ring with a wall. *Exp. Fluids* 12:41–8
Magarvey RH, Bishop RL. 1961a. Transition ranges for three-dimensional wakes. *Can. J. Phys.* 39:1418–22
Magarvey RH, Bishop RL. 1961b. Wakes in liquid-liquid systems. *Phys. Fluids* 4:800–5
Masuda N, Yoshida J, Ito B, Furuya T, Sano O. 2012. Collision of a vortex ring on granular material. Part I. Interaction of the vortex ring with the granular layer. *Fluid Dyn. Res.* 44:015501

Lubrication theory for a cylinder moving along a wall.

Merlen A, Frankiewicz C. 2011. Cylinder rolling on a wall at low Reynolds numbers. *J. Fluid Mech.* 685:461–94
Mittal R. 1999. Planar symmetry in the unsteady wake of a sphere. *AIAA J.* 37:388–90
Mittal S, Kumar B. 2003. Flow past a rotating cylinder. *J. Fluid Mech.* 476:303–34
Oertel H. 1990. Wakes behind blunt bodies. *Annu. Rev. Fluid Mech.* 22:539–64
Orlandi P, Verzicco R. 1993. Vortex rings impinging on walls: Axisymmetric and three-dimensional simulations. *J. Fluid Mech.* 256:615–46
Poon EKW, Ooi ASH, Giacobello M, Iaccarino G, Chung D. 2014. Flow past a transversely rotating sphere at Reynolds numbers above the laminar regime. *J. Fluid Mech.* 759:751–81
Pralits JO, Brandt L, Giannetti F.. 2010. Instability and sensitivity of the flow around a rotating circular cylinder. *J. Fluid Mech.* 650:513–36
Prasad A, Williamson CHK. 1997. The instability of the shear layer separating from a bluff body. *J. Fluid Mech.* 333:375–402
Prokunin AN. 2003. On a paradox in the motion of a rigid particle along a wall in a fluid. *Fluid Dyn.* 38:443–57
Prokunin AN. 2004. Microcavitation in the slow motion of a solid spherical particle along a wall in a fluid. *Fluid Dyn.* 39:771–8.
Rajamuni MM, Thompson MC, Hourigan K. 2018. Vortex-induced vibration of a transversely rotating sphere. *J. Fluid Mech.* 847:786–820.
Rao A, Stewart BE, Thompson MC, Leweke T, Hourigan K. 2011. Flows past rotating cylinders next to a wall. *J. Fluids Struct.* 27:668–79
Rao A, Passaggia P-Y, Bolnot H, Thompson MC, Leweke T, Hourigan K. 2012. Transition to chaos

in the wake of a rolling sphere. *J. Fluid Mech.* 695:135–48

Rao A, Thompson MC, Leweke T, Hourigan K. 2013a. The flow past a circular cylinder translating at different heights above a wall. *J. Fluids Struct.* 41:9–21

Rao A, Thompson MC, Leweke T, Hourigan K. 2015a. Flow past a rotating cylinder translating at different gap heights along a wall. *J. Fluids Struct.* 57:314–30

Rao A, Radi A, Leontini J, Thompson MC, Sheridan J, Hourigan K. 2015b. A review of rotating cylinder wake transitions. *J. Fluids Struct.* 53:2–14.

Reichl P, Hourigan K, Thompson MC. 2003. The unsteady wake of a circular cylinder near a free surface. *Flow Turbul. Combust.* 71:347–59.

Reichl P, Hourigan K, Thompson MC. 2005. Flow past a cylinder close to a free surface. *J. Fluid Mech.* 533:269–96.

Robichaux J, Balachandar S, Vanka SP. 1999. Three-dimensional Floquet instability of the wake of square cylinder. *Phys. Fluids A* 11:560–78

Ruiz-Angulo A, Hunt ML. 2010. Measurements of the coefficient of restitution for particle collisions with ductile surfaces in a liquid. *Granul. Matter* 12:185–91

Sareen A, Zhao J, Sheridan J, Hourigan K, Thompson MC. 2018. Vortex-induced vibrations of a sphere close to a free surface. *J. Fluid Mech.* 846:1023–58

Seddon JRT, Mullin T. 2006. Reverse rotation of a cylinder near a wall. *Phys. Fluids* 18:041703

Shao Y, Zhang Y-P, Zhu DZ, Zhang T-Q. 2013. Drag force on a free surface-piercing yawed circular cylinder in steady flow. *J. Fluids Struct.* 43:145–63

Sheard GJ. 2011. Wake stability features behind a square cylinder: Focus on small incidence angles. *J. Fluids Struct.* 27, 734–42

Sheard GJ, Thompson MC, Hourigan K, Leweke T. 2005. The evolution of a subharmonic mode in a vortex street. *J. Fluid Mech.* 534, 23–38

Sheard GJ, Leweke T, Thompson MC, Hourigan K. 2007. Flow around an impulsively arrested circular cylinder. *Phys. Fluids* 19, 083601

Sheridan J, Lin J-C, Rockwell D. 1997. Flow past a cylinder close to a free surface. *J. Fluid Mech.* 330:1-30.

Smart JR, Beimfohr S, Leighton DT. 1993. Measurement of the translational and rotational velocities of a non-colloidal sphere rolling down a smooth inclined plane at low Reynolds number. *Phys. Fluids A* 5:13–24

Smart JR, Leighton DT. 1989. Measurement of the hydrodynamic surface roughness of non-colloidal spheres *Phys. Fluids A* 1:52–60

Stewart BE, Hourigan K, Thompson MC, Leweke T. 2006. Flow dynamics and forces associated with a cylinder rolling along a wall. *Phys. Fluids* 18:111701

Stewart BE. 2008. *The dynamics and stability of flows around rolling bluff bodies*. PhD Thesis, Monash University/Université de Provence Aix-Marseille I

Stewart BE, Leweke T, Hourigan K, Thompson MC. 2008. Wake formation behind a rolling sphere. *Phys. Fluids* 20:071704

Stewart BE, Thompson MC, Leweke T, Hourigan K. 2010a. Numerical and experimental studies of the rolling sphere wake. *J. Fluid Mech.* 643:137–62

Stewart BE, Thompson MC, Leweke T, Hourigan K. 2010b. The wake behind a cylinder rolling on a wall at varying rotation rates. *J. Fluid Mech.* 648:225-56

Stojković D, Breuer M, Durst F. 2002. Effect of high rotation rates on the laminar flow around a circular cylinder. *Phys. Fluids* 14:3160–78

Stojković D, Schön P, Breuer M, Durst F. 2003. On the new vortex shedding mode past a rotating circular cylinder. *Phys. Fluids* 15:1257–60

Swearingen JD, Crouch JD, Handler RA. 2000. Dynamics and stability of a vortex ring impacting a solid boundary. *J. Fluid Mech.* 297:1–28

Taneda S. 1965. Experimental investigation of vortex streets. *J. Phys. Soc. Jpn.* 20:1714–21

Surveys of cylinder wake instability modes as function of rotation rate, with and without wall proximity, respectively.

First visualization of the wake of a cylinder moving parallel to a wall.

Tatsuno M, Taneda S. 1971. Visualization of the unsteady flow past cylinders and plates decelerated from a steady speed. *J. Phys. Soc. Jpn.* 31:1266–74

Taylor GI. 1963 Cavitation of a viscous fluid in narrow passages. *J. Fluid Mech.* 16:595–619

Terrington SJ, Hourigan K, Thompson MC. 2020. The generation and conservation of vorticity: deforming interfaces and boundaries in two-dimensional flows. *J. Fluid Mech.* 890: A5

Thompson MC, Leweke T, Provansal M. 2001. Kinematics and dynamics of sphere wake transition. *J. Fluid Struct.* 15: 575–86

Thompson MC, Hourigan K. 2005. The shear layer instability of a circular cylinder wake. *Phys. Fluids* 17:021702

Thompson MC, Hourigan K, Sheridan J. 1996. Three-dimensional instabilities in the wake of a circular cylinder. *Exp. Therm. Fluid Sci.* 12:190–6

Thompson MC, Hourigan K, Cheung, Leweke T. 2006a. Hydrodynamics of a particle impact on a wall. *Appl. Math. Mod.* 30:1356–69

Thompson MC, Hourigan K, Ryan K, Sheard GJ. 2006b. Wake transition of two-dimensional cylinders and axisymmetric bluff bodies. *J. Fluids Struct.* 22:793–806

Comprehensive study of the flow generated by the wall impact of a sphere.

Thompson MC, Leweke T, Hourigan K. 2007. Sphere-wall collisions: vortex dynamics and stability. *J. Fluid Mech.* 575:121–48

Tomboulides AG, Orszag SA. 2000. Numerical investigation of transitional and weak turbulent flow past a sphere. *J. Fluid Mech.* 416:45–73

Verekar PK, Arakeri JH. 2010 Sphere rolling down an incline submerged in a liquid. In *Proceedings of the 37th International & 4th National Conference on Fluid Mechanics and Fluid Power*, paper FMFP10-AM-01. Chennai: IIT Madras

Vlachos PP, Tellionis D. 2004. The effect of free surface on the vortex shedding from inclined circular cylinders. *ASME J. Fluids Engg* 130:021103

Walker JD, Smith CR, Cerra AW, Doligalski TL. 1987. The impact of a vortex ring on a wall. *J. Fluid Mech.* 181:99–140

Wang W, Dalton C. 1991. Numerical solutions for impulsively started and decelerated viscous flow past a circular cylinder. *Int. J. Numer. Methods Fluids* 12:383–400

Willetts B. 1998. Aeolian and fluvial grain transport. *Phil. Trans. R. Soc. Lond. A* 356:2497–513

Williamson CHK. 1989. Oblique and parallel modes of vortex shedding in the wake of a circular cylinder at low Reynolds numbers. *J. Fluid Mech.* 206:579–627

Williamson CHK. 1996a. Three-dimensional wake transition. *J. Fluid Mech.* 328:345–407

Williamson CHK. 1996b. Vortex dynamics in the cylinder wake. *Annu. Rev. Fluid Mech.* 28:477–539

Williamson CHK, Govardhan R. 2004. Vortex-induced vibrations. *Annu. Rev. Fluid Mech.* 36:413–55

Yildirim B, Yang H, Gouldstone A, Müftü S. 2017. Rebound mechanics of micrometre-scale, spherical particles in high-velocity impacts. *Proc. R. Soc. A* 473:20160936

Yoon H, Lee J, Seo J, Park H. 2010. Characteristics for flow and heat transfer around a circular cylinder near a moving wall in wide range of low Reynolds number. *Int. J. Heat Mass Trans.* 53:5111–20

Zeng L, Balachandar S, Fischer P. 2005. Wall-induced forces on a rigid sphere at finite Reynolds number. *J. Fluid Mech.* 536:1–25

Zeng L, Najjar F, Balachandar S, Fischer P. 2009. Forces on a finite-sized particle located close to a wall in a linear shear flow. *Phys. Fluids* 21:033302

Zhao Y, Galvin KP, Davis RH. 2002. Motion of a sphere down a rough plane in a viscous fluid. *Int. J. Multiph. Flow* 28:1787–800

Zhao J, Lo Jacono D, Sheridan J, Hourigan K, Thompson MC. 2018. Experimental investigation of in-line flow-induced vibration of a rotating circular cylinder. *J. Fluid Mech.* 847:664–99

Ziskind G. 2006. Particle resuspension from surfaces: revisited and re-evaluated. *Rev. Chem. Eng.* 22:1–123